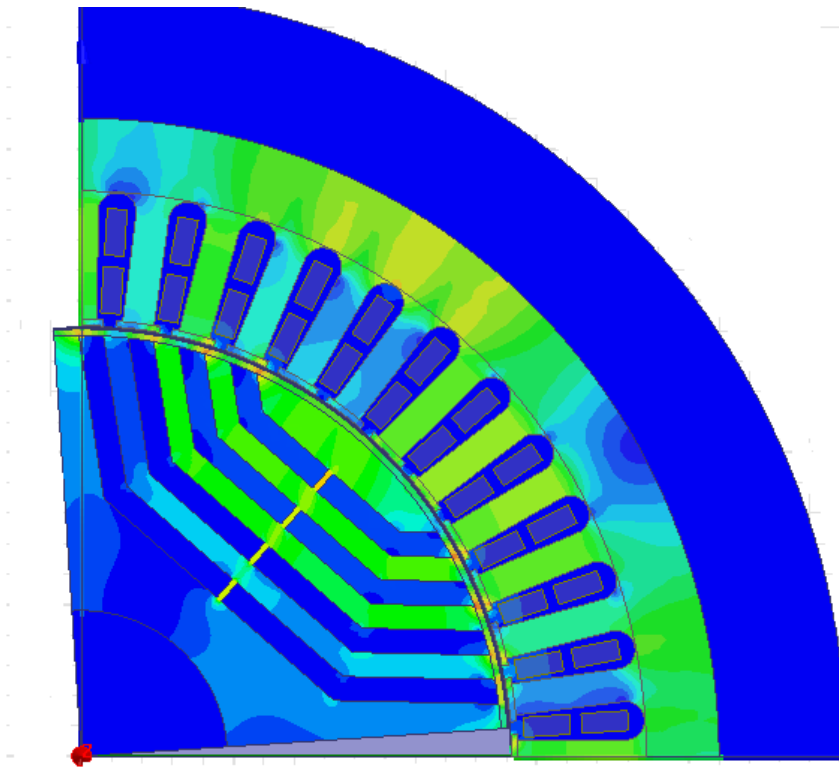




**CHALMERS**  
UNIVERSITY OF TECHNOLOGY

---



# Modeling and analysis of SynRM for hybrid electric vehicle application

Master's thesis in Electric Power Engineering

JOSIP ZEKIC



MASTER'S THESIS 2016

**Modeling and analysis of SynRM for hybrid  
electric vehicle application**

JOSIP ZEKIC



**CHALMERS**  
UNIVERSITY OF TECHNOLOGY

Department of Energy and Environment  
*Division of Electric Power Engineering*  
CHALMERS UNIVERSITY OF TECHNOLOGY  
Göteborg, Sweden 2016

Modeling and analysis of SynRM for hybrid electric vehicle application

JOSIP ZEKIC

© JOSIP ZEKIC, 2016.

Supervisor: Andreas Andersson, Volvo Car Group

Examiner: Professor Torbjörn Thiringer, Chalmers University of Technology

Master's Thesis 2016

Department of Energy and Environment

Division of Electric Power Engineering

Chalmers University of Technology

SE-412 96 Göteborg

Telephone +46 31 772 1000

Cover: Maxwell model showing magnetic flux in SynRM.

Chalmers Bibliotek, Reproservice

Göteborg, Sweden 2016

Modeling and analysis of SynRM for hybrid electric vehicle application  
JOSIP ZEKIC  
Department of Energy and Environment  
Division of Electric Power Engineering  
Chalmers University of Technology

## Abstract

In this thesis, the performance of a 4-pole SynRM is evaluated and compared to a reference 8-pole PMSM of the same size, where the machines are used in a hybrid electric vehicle (HEV) application. In order to perform a performance comparison between the machines, a design of the SynRM rotor is developed. The design is determined by using two different Mathematical Models that provides the size and position of the rotor air barriers and iron segments.

The final comparison between the SynRM and the PMSM shows that if the machines operates with the same current density in the stator windings, the average torque produced by the SynRM is approximately one third of the torque produced by the PMSM. If both machines are run with the same stator current, the average torque produced by the SynRM is slightly less than half of the torque in the PMSM and the torque ripple can be reduced to levels similar to the ones in the PMSM. The low performance is mainly due to rapid saturation along the d-axis, therefore, making the current angle one important factor. The efficiency is also slightly lower in the SynRM compared to the PMSM. As expected, when the machine is operated along the MTPA line, it shows improvement in efficiency and reduction in losses. The efficiency of the SynRM is only a few percent less than the efficiency of the PMSM.

Overall, more study is needed in the field, mainly to see how an increased size and proper control affects the system. But also to see what impact higher insulation ratios have on the machine. The alignment of the air barriers in the rotor against the stator slots is the single variable that effects the torque ripple the most. The SynRM also shows signs of saturation for low current, an issue that probably can be handled by the use of control strategies such as the MTPA combined with an increased rotor diameter. The saturation issue may also be reduced if it is being considered when developing a rotor design. Overall, the results in this thesis indicates that the SynRM is not a valid replacement for the PMSM in HEV applications with the design presented in this thesis.



## Acknowledgements

Initially, I would like to express my sincere gratitude to my supervisor Andreas Andersson and to my examiner Professor Torbjörn Thiringer for giving me this opportunity and for always providing help and guidance whenever it was needed. Also i would like to thank Pinar Tokat for providing good advice and ideas to during the realization of this work. They have all been one key factor in the realization of this thesis.

I would also like to express gratitude to my family for giving me this opportunity to study, expand my knowledge and for all their support and love.

Finally, I would like to thank Peter Andersson for letting me perform this work in his team at Volvo Car Group. I would also like to thank all my friends and colleges at Volvo Car Group for all the great discussions and ideas they have provided for this work.

Josip Zekic, Göteborg, May 2016



# Contents

<b>1</b>	<b>Introduction</b>	<b>1</b>
1.1	Aim of the thesis . . . . .	2
1.2	Method . . . . .	2
1.3	Project outline . . . . .	2
<b>2</b>	<b>The Electric Drives</b>	<b>3</b>
2.1	Basic Electromagnetic Theory . . . . .	3
2.2	The Permanent Magnet Synchronous Motor . . . . .	4
2.3	The Synchronous Reluctance Motor . . . . .	5
2.3.1	The concept of reluctance . . . . .	6
2.3.2	Characteristics of the SynRM . . . . .	7
2.3.2.1	Voltage equations . . . . .	7
2.3.2.2	Torque characteristics and equations . . . . .	8
2.3.2.3	Saliency ratio and Power factor . . . . .	9
2.3.2.4	Power losses and Efficiency . . . . .	10
2.3.3	The SynRM Rotor . . . . .	11
2.3.3.1	Flux Barriers and Segments . . . . .	12
2.3.3.2	Insulation ratio . . . . .	13
2.3.4	Air gap length . . . . .	13
<b>3</b>	<b>The SynRM Rotor Design Parameters and Procedure</b>	<b>15</b>
3.1	Mathematical Model 1 . . . . .	15
3.1.1	Segment width . . . . .	16
3.1.2	Air barrier width . . . . .	17
3.2	Mathematical Model 2 . . . . .	18
3.2.1	Segment Width . . . . .	19
3.2.2	Air barrier width . . . . .	20
<b>4</b>	<b>Case Setup</b>	<b>23</b>
4.1	Target Parameters . . . . .	23
4.2	Time steps and meshing . . . . .	23
4.3	The SynRM Simulation Setup . . . . .	25
4.4	The PMSM Simulation setup . . . . .	27
<b>5</b>	<b>Analysis</b>	<b>29</b>
5.1	The SynRM Initial Model . . . . .	29
5.1.1	Mathematical Model 2 - S1 Selection . . . . .	29

5.1.1.1	S1 selection - Analysis . . . . .	31
5.1.2	Model Comparison - Torque Performance . . . . .	32
5.1.3	Model Comparison - Losses . . . . .	37
5.1.4	Model Comparison - Saliency Ratio & Efficiency . . . . .	39
5.1.5	Model Comparison - Analysis . . . . .	43
5.2	SynRM Asymmetric Ripple Reduction . . . . .	44
5.2.1	Asymmetric Design - Analysis . . . . .	45
5.3	SynRM Final Design - Case analysis . . . . .	48
5.4	SynRM & PMSM comparison . . . . .	53
5.4.1	Reference - Current Density . . . . .	54
5.4.2	Reference - Current . . . . .	56
5.4.3	SynRM with MTPA . . . . .	59
5.4.4	Final Analysis . . . . .	60
<b>6</b>	<b>Conclusion</b>	<b>63</b>
6.1	Conclusions . . . . .	63
6.2	Future Work . . . . .	64
	<b>Bibliography</b>	<b>65</b>

# 1

## Introduction

As governments introduce more restrictions and regulations against internal combustion engines (ICE) cars and tax reductions for Hybrid Electric Vehicles (HEV), the hybrids have increased in popularity. Ever since manufacturers such as Tesla Motors Inc. have entered the market, their sales figures have shown that the market is accepting the concept of electric vehicles. The HEV usually use a combustion engine and an assisting electric motor to propel the vehicle. The combustion engine may also work as a range extender, more specifically as a generator harvesting energy for the vehicles' batteries'. Pure electric vehicles, i.e. battery electric vehicles (BEV), only use electric motor(s) to propel the vehicle and therefore lack the ICE. The BEV and HEV possess many benefits compared to the ICE cars, such as high energy efficiency and reduced fuel costs. As for conventional ICEs', the electric motors used in BEVs and HEV come in different shapes and types. One of the most widely used machine topologies to date in HEV are the Permanent Magnet Synchronous Machines (PMSM)[1]. The PMSM has high efficiency and high torque & power density, thereby making it a commonly used electric motor in a HEV [1]. A disadvantage of the PMSM is that it uses rare earth materials for the magnets, which can vary in cost. By excluding the rare earth magnets from the rotor, the motor unit price can be reduced. This means that by replacing the PMSM with a SynRM the price of the motor can be reduced by approximately 25% [2][3]. The SynRM is known to have a lower power and torque density compared to the PMSM, as a consequence of the absence of permanent magnets in the rotor.

This leads to the question of how much difference there is in torque, torque ripple, efficiency and power density between the two motors. One of the main reasons to study the SynRM in HEV and BEV applications is to find out if the difference in these properties is small enough to consider the SynRM as a valid alternative to the PMSM. By evaluating the difference in the properties mentioned above, the loss can perhaps be compensated by the lower unit price of the SynRM. If packaging in the HEV or BEV allows, the size of the SynRM may be increased in order to compensate for losses in torque, power density and the rest of the aforementioned properties. This leads to that different designs of the SynRM should be evaluated and compared to the PMSM in order to provide more information on the possibilities of the SynRM as the main propulsion unit in HEV & BEV applications.

## 1.1 Aim of the thesis

The main aim of this thesis is to design a rotor of a 4-pole SynRM for use in BEV or HEV applications and compare it to an 8-pole reference PMSM. In order to achieve this, a suitable design needs to be developed with a proper analysis of the background theory and a mathematical model for providing the rotor design. Every suggested rotor design needs to be evaluated in terms of relevant target parameters, such as average torque, torque ripple, efficiency and power losses. From this, a rotor design can be selected and finally compared to the reference PMSM using the same current supply and current density for both machines.

## 1.2 Method

The modelling and evaluation of different rotor designs is done with ANSYS Maxwell 16.1. The aim is also to study and understand the impact on the performance of different design parameters. Such design parameters can be air-barrier width, barrier angle, air gap length and moreover. Once the final rotor design of the SynRM have been selected, it needs to be evaluated and compared against a provided reference PMSM. This is done for the same point of operation and where the reference motor is also evaluated in ANSYS Maxwell. The reference PMSM is a 8-pole machine which shares the stator with the SynRM. Since the reference motor is a 8-pole machine the stator windings will differ between the two machines. Once the performance of both of the machine has been evaluated, hopefully enough knowledge have been collected in order to be able to analyse and determine if the SynRM can be a viable replacement for the PMSM in HEV applications.

## 1.3 Project outline

This thesis is divided into 6 different chapters. The first chapter brings a short introduction to the subject of electric machines in HEV applications and some primary goals of the project. The second chapter provides the reader with some useful background theory related to electromagnetics, the two machine topologies used in this thesis, i.e. the PMSM and the SynRM. The third chapter will present two different mathematical models that are being used to find a suitable design of the rotor and its air barriers. The first mathematical model is identical to the one presented in [6]. The second mathematical model is specifically developed for this study. With the help of these mathematical models suggestions are made for size and position of different design elements, such as air barriers and iron segment widths. The fourth chapter presents the simulation setups that have been used in this work. Some key elements, such as meshing, time stepping and stator windings are presented in this section. The fifth chapter contains the analyses and the results. The final sixth chapter contains the main conclusions for this study and also some suggestions for future work.

# 2

## The Electric Drives

The electrical drives systems can vary in shape and setup and are usually divided into DC drives and AC drives. This project focuses mainly on the Synchronous Reluctance Machine (SynRM) but also on the Permanent Magnet Synchronous Machine (PMSM) and since both of these are similar in functionality, most of the underlying theory can be derived from basic electromagnetic theory. The aim of this chapter is to provide the necessary understanding of the underlying electromagnetic theory explaining the operation and design of the PMSM and the SynRM.

### 2.1 Basic Electromagnetic Theory

To achieve greater understanding of the operation of the electric drives it is useful to study the basic electromagnetic theory. By applying a conductor winding around an iron core with an air gap, a magnetic field is generated in the air gap. The flux created by the winding can be written as

$$\Phi = \iint B dS \quad (2.1)$$

where  $B$  is the flux density of the magnetic field measured in Tesla and  $dS$  is the area of the iron core from which the flux exits. With knowledge of the current direction, the direction of the field may also be obtained meaning that the correlation between the enclosed current in the coil, current density and the magnetic flux density can be written as

$$I_{encl} = \oint \frac{B}{\mu} dl = \iint J_v dS \quad (2.2)$$

where  $J_v$  is the current density ( $A/m^2$ ) and  $\mu$  is the permeability of the material. It is worth pointing out that the permeability of a material is written as a product of relative permeability of a material,  $\mu_r$  and the permeability of free space,  $\mu_0$ . This is essential since the relative permeability can vary largely between materials. In a solid iron core the permeability can reach up to 10 000 ( $A/m$ ) compared to approximately 1( $A/m$ ) for air [9]. The result of this difference is that the field intensity is higher in the air gap than in the iron core, thus showing that lower permeability results in a stronger field. In electric drives applications there is one parameter of extra interest, namely the flux linkage  $\Psi$ . By applying Faraday's Law of Induction the induced electromotive force (emf) can be written as the negative time derivative of the total flux linkage, demonstrated below

$$e_m = -\frac{d\Psi}{dt} \quad (2.3)$$

One central parameter when studying the performance of a SynRM is the inductance. The inductance in an electromagnetic circuit can be written as

$$L = \frac{\Psi}{I} \quad (2.4)$$

showing the correlation between the magnetic flux linkage  $\Psi$ , the current  $I$  and the inductance  $L$ . The winding in the circuit does consist of a real and an imaginary part, meaning that the winding contains both a resistive component and an inductive component. This will cause a voltage drop over the winding and the voltage can be written as

$$v = L\frac{di}{dt} + Ri \quad (2.5)$$

where  $R$  is the resistance of the wire [9]. By inserting a magnet in the air gap of the u shaped iron, the magnet will begin to rotate in the field with an angular speed of  $\omega_r$  and thereby the most basic operation of an electrical motor is demonstrated. The voltage equation can now be written as a combination of the elements above

$$v = L\frac{di}{dt} + Ri + \omega_r\Psi_m \cos(\omega_r t) \quad (2.6)$$

thus resulting in an applicable expression for electric machines [9].

## 2.2 The Permanent Magnet Synchronous Motor

The PMSM are commonly used in HEV applications and can serve both as the main propulsion motor or as starters/alternators. It offers several beneficial properties, such as high efficiency and no internal windings [9]. The high efficiency is achieved by the utilization of both reluctance and magnetic torque and reduction in resistive losses [1]. At high speeds the PM-generated flux needs to be counteracted in order to limit the back-emf. This is typically done by enforcing a high current in the negative d-axis [1]. The PMSM will be used as a reference machine in this work due to its similarities with the SynRM. The equations for the SynRM can be derived directly from those of the PMSM. It is therefore useful to do a brief analysis of the characteristic of the PMSM. The voltage equations for the stator in the d-q reference frame can initially be written as [9]

$$v_{sd} = R_s i_{sd} + L_{sd} \frac{di_{sd}}{dt} - \omega_r L_{sq} i_{sq} \quad (2.7)$$

$$v_{sq} = R_s i_{sq} + L_{sq} \frac{di_{sq}}{dt} + \omega_r L_{sd} i_{sd} + \omega_r \Psi_m \quad (2.8)$$

where  $R_s$  is the stator winding resistance and  $\Psi_m$  the magnetic flux linkage constant. Since it is easier to control DC-voltage compared to AC-voltage, it is common

practice to express the electrical equations of the stator voltage in rotating reference frame, i.e in the d-q plane for steady state. This means that the voltage can be expressed as two DC voltages,  $v_d$  and  $v_q$ . In steady state, the the time derivative is equal to zero and (2.7) and (2.8) can be rewritten as

$$v_{sd} = R_s i_{sd} - \omega_r L_{sq} i_{sq} \quad (2.9)$$

$$v_{sq} = R_s i_{sq} + \omega_r L_{sd} i_{sd} + \omega_r \Psi_m. \quad (2.10)$$

The inductance's in d & q direction can be calculated with the knowledge of the magnetic flux linkage  $\Psi_m$  and the flux linkage in d & q direction,  $\Psi_d$  and  $\Psi_q$ . This means that the inductance's  $L_d$  and  $L_q$  can be expressed as[9]

$$L_d = \frac{\Psi_d - \Psi_m}{i_{sd}} \quad (2.11)$$

$$L_q = \frac{\Psi_q}{i_{sq}} \quad (2.12)$$

Since the PMSM contains permanent magnets in the rotor, the torque will be product of both magnet torque and reluctance torque. This means that the torque production for a PMSM can be written as

$$T_e = \frac{3n_p}{2} (\Psi_m i_{sq} + (L_{sd} - L_{sq}) i_{sd} i_{sq}) \quad (2.13)$$

## 2.3 The Synchronous Reluctance Motor

The lack of permanent magnets have made the SynRM an interesting alternative to the PMSM and the Induction Machine (IM) in various applications. However, there are some drawbacks to the concept. Already in 1923, Kostko showed that there were some limitations to the performance of the SynRM. This as a result of low salency ratio and the lack of possibility of a direct on line (DOL) start of the machine [4]. As improvements of converters have created possibilities to control voltage and frequency to the machine more efficient, improvement of the overall performance, power density and power factor have been achieved[7]. The SynRM is similar in design to the PMSM, but consists of a salient rotor without magnets. In general, it can be stated that the SynRM have several beneficial properties, some being high efficiency and high torque per ampere capability[17]. The absence of windings in the rotor reduces the overall heat production of the SynRM and PMSM meaning that both are especially suitable for automotive applications from this perspective[11]. Despite the beneficial properties mentioned above, it is essential to point out some

of the drawbacks of the SynRM. High torque ripple, low power factor and the need of a small air gap all contributes to the limited use of the SynRM in vehicles[17].

### 2.3.1 The concept of reluctance

The idea of reluctance torque production in electric machines have been a long discussed topic and stretches back to the beginning of the 20th century. In similarity with the PMSM, the SynRM uses a sinusoidally rotating MMF produced by the stator, therefore, the use of the same stator in both machines is fully possible [5]. As in the case of the PMSM, it is common practice to mathematically describe the SynRM in the rotating reference plane, i.e in the direct and quadrature axes. By inserting an object into the magnetic field, the object will naturally seek alignment with the field and thereby reluctance torque is created, which rotates the object in the field. The phenomenon of reluctance torque is shown in Figure 2.1. The stator current in the SynRM is producing the field by windings distributed in the stator slots, meaning that there is no current passing through the rotor. Therefore, the only link between rotor and stator is through the magnetic field via the small air gap. Since the rotor does not produce an field by its own, it will try to align itself with the sinusoidal magnetic field created by the stator. Once the rotor have aligned with the rotation of the stator magnetic field, the rotor is thereby rotating at a synchronous speed [6].

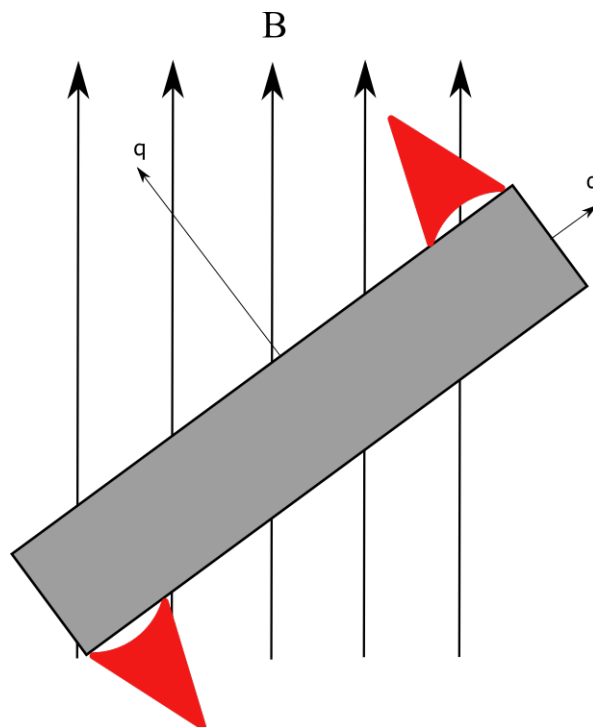


**Figure 2.1:** Object placed in a magnetic field, showing how reluctance torque creates the rotation of the object.

### 2.3.2 Characteristics of the SynRM

The SynRM have some key characteristics that defines the actual behaviour of the machine. Torque, saliency ratio, power factor, efficiency and losses are all key parameters directly related to the performance of the machine[17]. To further understand the behaviour of the SynRM, analysing these in depth is useful.

#### 2.3.2.1 Voltage equations

It is common to describe the electrical characteristics of the SynRM in the d-q plane from rotor reference, meaning that the machine's terminal stator voltage  $V_s$  and stator current  $i_s$  can be expressed as voltage and current components in the d-q plane

$$V_s = v_{sd} + jv_{sq} \quad (2.14)$$

$$i_s = i_{sd} + ji_{sq}. \quad (2.15)$$

The main equations for the SynRM in the d-q plane, can be derived directly from the PMSM equations by excluding the magnetising components. From these, the voltage equations of the SynRM can be written as

$$v_{sd} = R_s i_{sd} + L_{sd} \frac{di_{sd}}{dt} - \omega_r L_{sq} i_{sq} \quad (2.16)$$

$$v_{sq} = R_s i_{sq} + L_{sq} \frac{di_{sq}}{dt} + \omega_r L_{sd} i_{sd}. \quad (2.17)$$

In (2.16) and (2.17)  $R_s$  is the stator winding resistance and  $\omega_r$  is the rotor angular speed. Since the inductances,  $L_d$  and  $L_q$ , in general contains both mutual and leakage components,  $L_d$  and  $L_q$  can therefore be rewritten as [5]

$$L_d = L_{\sigma s} + L_{md} \quad (2.18)$$

$$L_q = L_{\sigma s} + L_{mq} \quad (2.19)$$

where,  $L_{\sigma s}$ , is the leakage inductance component and,  $L_{md}$ ,  $L_{mq}$ , the mutual inductance components. The flux linkage can be expressed as product of the current and the inductance and can be expressed as

$$\Psi_d = L_d i_d \quad (2.20)$$

$$\Psi_q = L_q i_q. \quad (2.21)$$

Due to the dependency of both d and q current on the mutual flux linkage, the non-linear effect of cross coupling is expected to be major and therefore it needs to be mentioned. However, the effect of cross coupling can be overseen from a modeling perspective and is therefore to greater importance when designing a controller of the machine. It is also worth point out that the terms  $\frac{d\Psi_d}{dt}$  and  $\frac{d\Psi_q}{dt}$  is equal to zero during steady state operation[17]. Therefore, a valid use-able mathematical model of the d and q-axis components of (2.14) can be written as

$$v_{ds} = R_s i_{ds} - \omega L_q i_{qm} \quad (2.22)$$

$$v_{qs} = R_s i_{qs} + \omega L_d i_{dm}. \quad (2.23)$$

Due to the possibility to assume that measurements of  $L_d$  and  $L_q$  are being accurate enough, (2.22) and (2.23) can be used for modelling purposes[10].

### 2.3.2.2 Torque characteristics and equations

The torque of the SynRM is being created by the difference in inductance between the direct and the quadrature axes. More specific, by the  $(L_d - L_q)$  term. A higher difference between  $L_d$  and  $L_q$  the greater the effect on the torque. Given that  $L_d \neq L_q$ , the torque of the SynRM for  $n_p$  pole pair can initially be expressed as

$$T_e = \frac{3}{2} n_p (L_d - L_q) i_{ds} i_{qs}. \quad (2.24)$$

Using (2.18) and (2.19) the torque equation (2.24) can be rewritten in terms of the machines mutual components. The mutual current  $i_m$  will be smaller than the stator current  $i_s$  since  $i_m = i_s - i_\sigma$ . Since it is the mutual current components that actually produces the torque, the torque can be rewritten as [20]

$$T_e = \frac{3}{2} n_p (L_{md} - L_{mq}) i_{qm} i_{dm}. \quad (2.25)$$

It should be mentioned that the torque equation of the SynRM can be written in several different ways [17]. One different denotation of the torque equation can be written as

$$T_e = \frac{3}{2} n_p (L_{md} - L_{mq}) i_m^2 \sin(2\theta) \quad (2.26)$$

where the torque is dependent on the squared mutual current  $i_m$  and on the current angle  $\theta$ . The current angle is the angle between the d-axis and  $i_m$ . The benefit of expressing the torque in terms of  $\theta$  is due to the possibility to control the current angle during control of the machine [17].

One other important characteristic of the machine is the torque ripple. It is one of the main properties of the machine and therefore it needs to be mentioned. Achieving reduced torque ripple still remains one of the biggest challenges when designing the SynRM and there have been several studies on this topic. One way to express the torque ripple is simply [19]

$$T_{rip} = \frac{(T_{max} - T_{min})}{T_{avg}}. \quad (2.27)$$

### 2.3.2.3 Saliency ratio and Power factor

One of the important performance parameters is the inductance ratio, more specific the ratio between the d-axis inductance and the q-axis inductance [13]. This ratio is also referred to as saliency ratio, often denoted as

$$\xi = \frac{L_d}{L_q} \quad (2.28)$$

The saliency ratio provides a general indication of the overall performance because the power factor, several aspects of the dynamic response and more, are directly related to the saliency ratio [18]. In terms of the power factor of the machine, it is essential to differ between the internal power factor (IPF) and the terminal power factor (TPF) [17]. The IPF can be written on several different way, depending on parameters of interest and choice of control strategy [13]. One convenient way to express the IPF is in terms of both  $\xi$  and the current angle  $\theta$ , referring to the Maximum Torque Per kilo Volt Ampere (MTPkVA) strategy, is as follows [18][13]

$$IPF = (\xi - 1) \sqrt{\frac{\sin 2\theta}{2(\tan \theta + \xi^2 \cot \theta)}} \quad (2.29)$$

It must however be pointed out that (2.29) is valid only for motors with larger ratings, motors used in electric vehicles for instance. For motors with small rating the phase resistance cannot be approximated to zero, thereby invalidating (2.29), as discussed in [18]. The machine will reach its power factor peak when  $\theta = \arctan \sqrt{\xi}$  and using this argument in (2.29) gives that the maximum IPF can be written as [13]

$$IPF_{max} = \frac{(\xi - 1)}{(\xi + 1)} \quad (2.30)$$

It becomes evident from (2.30) that in order to achieve a high IPF, a high saliency ratio is required [15]. The correlation between the saliency ratio and the maximum IPF is shown in Fig. 2.2, thereby demonstrating the non linear effect that the saliency have on the growth of the IPF.

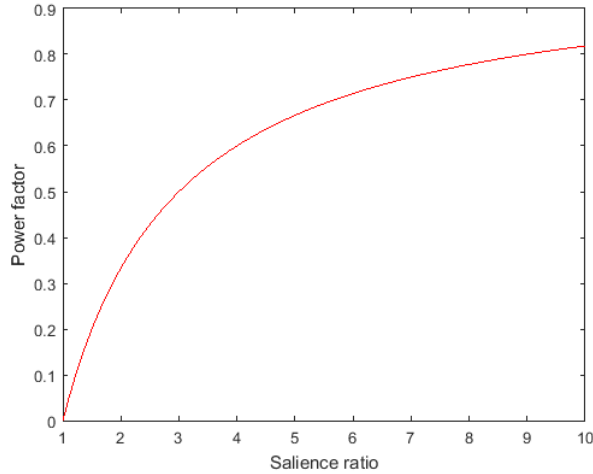


**Figure 2.2:** The correlation between the saliency ratio and IPF

Worth pointing out is that for saliency ratios higher than 7, the increase in power factor is leveling out. An increase of 100 percent in saliency ratio, i.e from 7 to 14, will only result in a gain of approximately 20 percent in power factor[16].

#### 2.3.2.4 Power losses and Efficiency

The losses in the SynRM that will be considered in this study can be divided into copper losses  $P_c$  and into iron losses  $P_i$  [19]. The iron losses are in general significantly smaller than the copper losses during low speed operations, but this assumption is not valid in high speed operations due to the iron losses direct dependency on frequency [17][21]. The losses in the SynRM used in this thesis can be written as

$$P_l = P_c + P_i. \quad (2.31)$$

The copper losses in the SynRM can, as discussed in [19], be expressed as

$$P_c = \frac{R_s}{3}(i_{ds}^2 + i_{qs}^2). \quad (2.32)$$

The more complex nature of the iron losses,  $P_i$ , will be dependent on several factors. Based on the Bertotti model, the iron losses can be divided into (i) Hysteresis losses, (ii) Eddy current losses and (iii) High frequency losses [21]. The Bertotti model shows how the frequency affects the iron losses and by applying it, the iron losses can be written as

$$P_i = P_h + P_{ec} + P_{hf} \quad (2.33)$$

where  $P_h$  are the hysteresis losses,  $P_{ec}$  are the eddy current losses and  $P_{hf}$  are the high frequency losses. The Bertotti model shows that (2.33) can be expressed as

$$P_i = K_h f B_m^2 + K_{ec} f^2 B_m^2 + K_{hf} f^{1.5} B_m^{1.5} \quad (2.34)$$

where  $K_h$  is the hysteresis loss factor,  $K_{ec}$  the eddy current loss coefficient and  $K_{hf}$  the high frequency loss coefficient. The methodology behind the extraction of these parameters can be found in detail in [22].

Directly dependent on the power losses is the efficiency of the machine, an important property particularly in electric vehicles applications [17]. This means that losses need to be minimized in order to keep an higher efficiency. One way to write the efficiency (neglecting surface and mechanical losses) is as

$$\eta = \frac{P_{in} - (P_c + P_i)}{P_{in}} \quad (2.35)$$

where  $P_{in} = P_{shaft} + P_{total}$ . The total losses are expressed as  $P_{total} = P_c + P_i$  and the mechanical shaft power is  $P_{shaft}$ . The shaft power is simply written as

$$P_{shaft} = T_e \omega_r \quad (2.36)$$

### 2.3.3 The SynRM Rotor

The rotor of the SynRM is one key component that will affect the performance of the machine significantly. Several studies have therefore been done on different topologies and layouts of the rotor. The structure of the rotor can be divided into three commonly used topologies as shown in Fig. 2.3[6][11]

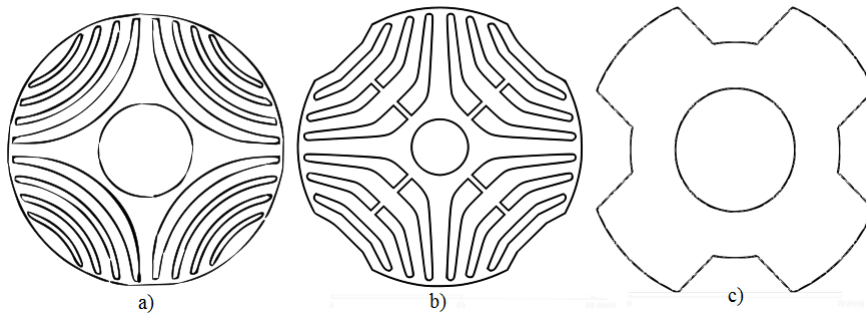


**Figure 2.3:** a) Axially laminated anisotropy (ALA), b) Transversely laminated anisotropic (TLA), c) Salient pole layout

The most basic, the salient pole layout, has been proven to have insufficient performance compared to other AC machines [11]. Low saliency ratio and low power factor are some properties of the salient pole rotor, something Kostko demonstrated in 1923 [4], but also later by [6]. It was shown that the widening of the cut-off barrier in-between the poles in order to reduce the q-axis inductance, resulted in unwanted reduction of d-axis inductance as well. The reduction in d-axis flux is an unwanted effect, which is due to the reduction of iron in the pole arc. Kostko concluded that a multi-barrier type layout, with no pole-arc reduction is the preferred layout for the SynRM rotor [4][13]. Given the low performance of the salient pole rotor, this

design is not considered in the present work.

An initial step is to study the field lines in a solid rotor and in Fig. 2.4 the dispersion of the field lines for one pole in a solid rotor is shown as hyperbolic lines. Therefore this becomes an indicator on what shape the flux barriers should obtain. The main purpose of the flux barriers is to reduce the q-axis flux in such a way that the d-axis flux remains as unaffected as possible [13]. By looking at (2.25) it can be seen that in order to maximize the torque,  $L_d$ , should stay as large as possible while,  $L_q$ , should be reduced to a minimal possible value. Due to the more complicated rotor structure of the ALA, its mechanical stress and production disadvantages, the TLA rotor structure is the most widely adopted and will also be used in this study[11].

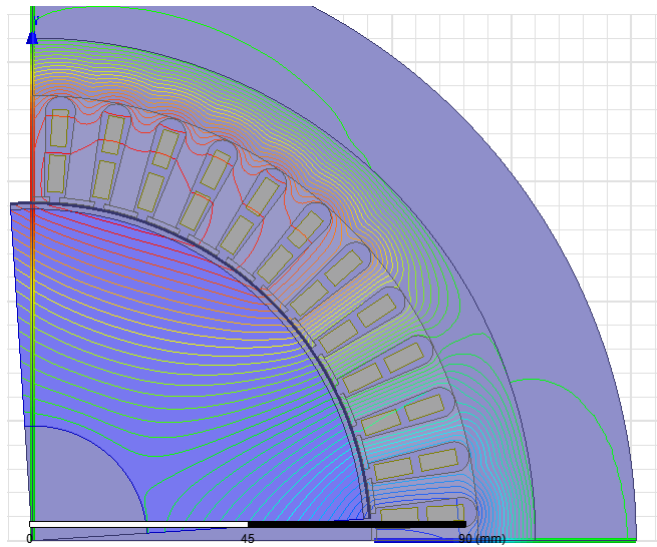


**Figure 2.4:** Magnetic flux lines in a solid rotor for one pole in a 4-pole SynRM.

### 2.3.3.1 Flux Barriers and Segments

Introducing the flux barriers in the rotor is a necessary step for increasing the d-axis inductance[6]. When designing the flux barriers there is some key aspects that are of special importance. The number of flux barriers, width of the flux barriers in q and d-direction, shape of the flux barriers and finally slot pitch angle[11].

Kostko shows that the use of only one flux barrier does not improve the performance of the motor sufficiently, compared to the salient pole layout [4]. Therefore, several studies have been conducted in order to find a more suitable number of flux barriers [11][14][13]. Studies have suggested that the increase of flux barriers leads to an improved canalization of the flux in the rotor, hence a improvement in performance [11][14][13]. Ideally in theory, the number of flux barriers should be as high as possible, in order to maximize the torque and to reduce the torque ripple [6]. However, due to mechanical structure and manufacturing limitations, there is a limit to the number of flux barriers.

The machine torque is directly proportional to the difference in inductance between d-axis and q-axis, i.e.  $(L_d - L_q)$ . The power factor of the machine is directly dependent on the saliency ratio, as shown earlier. In [13], Moghaddam shows that the difference in torque between four flux barriers and five flux barriers is small. Therefore, having five flux barriers or more, is assumed to result in only minor improvements to the performance of the machine. This value may, however depend, on the specific case and is therefore only used as an indication rather than a rule in this study. Furthermore, some studies suggest that if the number of flux barriers is greater than three, a saliency ratio of around 10 can be reached if the machine is not saturated, due to improved canalization of the flux [11].

### 2.3.3.2 Insulation ratio

One key parameter in the rotor design is the ratio between the amount of iron and air in the rotor. This parameter is referred to as insulation ratio [6]. The ratio implies that, if there is an equal amount of iron and air in the rotor, the ratio will be 1. The insulation ratio is sometimes divided into two different categories, one in d-axis direction and one in q-axis direction, but for this study only q-direction will be considered. This means that the barriers will have the same width in both q-axis and d-axis direction. By letting the total available length of iron, in radial direction, in the rotor along the q-axis be  $l_y$ , and the length of the air be  $l_a$ , the insulation ratio is simply

$$K_{wq} = \frac{l_a}{l_y}. \quad (2.37)$$

### 2.3.4 Air gap length

One important design aspect related to the rotor is the air gap length between the rotor and the stator. This is due to the fact that the air gap will have considerable effect on the inductances,  $L_d$ , and,  $L_q$  [16]. This behaviour is a result of the cross magnetisation between the d-axis and  $L_q$  and q-axis  $L_d$ . Thus, the air gap should be as small as possible in order to achieve a high saliency ratio and thereby a high difference in inductance [16]. Worth pointing out is the mechanical and manufacturing limitations when trying to achieve small air gaps and barriers. This is an important aspect when considering the final design of the SynRM in practice.



# 3

## The SynRM Rotor Design Parameters and Procedure

In order to be able to evaluate different designs and geometries in the rotor effectively it is useful to create a mathematical model for this purpose. Only sweeping between different designing geometries is a time consuming and noneffective approach. By introducing a mathematical model which aims on providing a suggestion for an initial design, the sweeping process can be conducted more effectively. When designing the air barriers there are several parameters and effects that needs to be considered. Finding the optimum design layout can therefore become a very complex task. In the present study, two different mathematical design model are presented. This chapter aims on providing a more detailed insight in the mathematical models behind the selection of the rotor design parameters that are used in the present study.

### 3.1 Mathematical Model 1

There have been several studies conducted in this field, trying to find a suitable model describing the positioning and dimensions of the air barriers and iron segments [6][13][23]. As a basis for the first mathematical model for this study, the mathematical design model derived in [6] will be used. It is briefly described and slightly modified to suit the prerequisites for this study. The full derivation of the model can be found in [6].

Before introducing the parameters that will be used to dimension the barriers, it is useful to look at the magnetic flux in the rotor and the induced MMF in the air gap. The MMF in the air gap consists of a component in the d-axis (MMFd) and a component in the q-axis (MMFq). In general, it can be said that the rotor have maximum reluctance in the d-axis and minimal reluctance in the q-axis [6]. One common design rule is to let the d-axis flux component pass throughout the whole rotor to maximise the magnetizing inductance. This means that the q-axis flux need to be reduced. Since the d-axis component of the magnetic flux will be passing through the entire rotor pole, therefore, it is common practice to align the d-axis with the magnetic flux, as demonstrated in Fig. 3.1 [6].

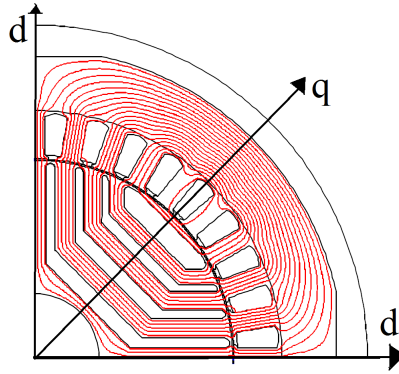


**Figure 3.1:** Magnetic flux distribution of the d-axis flux component for one pole in a SynRM

### 3.1.1 Segmenth width

By studying Figure 3.1 one can see that the flux path of the d-axis flux only consists of iron and the air gap. Since the the iron is a material of high permeability, the magnetic potential drops in the air gap. It can be seen that there is a correlation between the MFF and the iron segments position and size. To dimension the segments in the rotor, some parameters need to be introduced. The first parameter that is being considered is the slot pitch angle,  $\alpha_m$ . The slot pitch angle can be expressed as a function of number of barriers,  $k$ , pole pairs number,  $n_p$ , and an extra added necessary angle called,  $\beta$ , such as

$$\alpha_m = \frac{\left(\frac{\pi}{2n_p} - \beta\right)}{\left(k + \frac{1}{2}\right)}. \quad (3.1)$$

With the knowledge of the slot pitch angle, the angle,  $\beta$ , can be calculated. The main purpose of,  $\alpha_m$ , and,  $\beta$ , is to decide the distance between two so called endpoints. These barrier endpoints are the calculated endpoints of the barrier in the rotor. It is worth pointing out that the segment in-between two endpoints can contain both iron segment and air barriers. This is illustrated in detail in [6]. It is from these endpoints that the dimension and locations of iron segments are calculated. According to [6], one convenient starting point is to study the MMFd. It can be shown that the p.u MMF supplying the  $h^{th}$  segment,  $f_{dh}$ , is proportional to the h-th segment width (in q-axis direction),  $S_h$ [6]. The MMF supplying each segment,  $f_{dh}$ , can be calculated by taking an average of the MMF in-between two endpoints. This gives an expression as a ratio between the average MMF supply in p.u for the corresponding segments, as demonstrated below[6].

$$\frac{2S_1}{S_2} = \frac{f_{d1}}{f_{d2}} \quad (3.2)$$

$$\frac{S_h}{S_{h+1}} = \frac{f_{dh}}{f_{d_{h+1}}}, (h = 2, \dots, k) \quad (3.3)$$

The average MMF  $f_{dh}$  and segment width  $S_h$  are calculated from the following expressions

$$f_{dh} = \frac{\sin\left(n_p \frac{(2h-1)}{2} \alpha_m\right) - \sin\left(n_p \frac{(2h-3)}{2} \alpha_m\right)}{n_p \alpha_m} \quad (3.4)$$

$$f_{d_{k+1}} = \frac{1 - \sin\left(n_p \frac{(2h-1)}{2} \alpha_m\right)}{n_p (\alpha_m + \beta)}. \quad (3.5)$$

Applying a brief analysis of the equations above, it becomes evident that there are  $k$  equations but the number of unknown variables is  $k + 1$ . Therefore, another equation needs to be introduced. By using the insulation ratio along the q-axis, the total length of iron and air along the q-axis is given according to

$$K_{wq} = \frac{l_a}{l_y} \quad (3.6)$$

where,  $K_{wq}$ , is the insulation ratio,  $l_a$ , is the amount of air,  $l_y$ , is the amount of iron in q-axis direction and can be written as

$$l_a = \left(R_{rotor} - R_{shaft}\right) - \sum_{h=1}^{k+1} S_h \quad (3.7)$$

$$l_y = \sum_{h=1}^{k+1} S_h. \quad (3.8)$$

With the knowledge of the sum of all iron segments, each segment length can separately be calculated.

### 3.1.2 Air barrier width

As in the case with the segment width, the air barrier widths can be extracted from the MMF difference over each barrier [6]. The aim is to find a barrier size which will minimize the q-axis component flux. According to [6], the average MMF over each segment can be written as

$$f_{q1} = 0 \quad (3.9)$$

$$f_{qh} = \frac{\cos\left(n_p \frac{(2h-3)}{2} \alpha_m\right) - \cos\left(n_p \frac{(2h-1)}{2} \alpha_m\right)}{n_p \alpha_m}, (h = 2, \dots, k) \quad (3.10)$$

$$fq_{k+1} = \frac{\cos\left(n_p \frac{(2h-1)}{2} \alpha_m\right)}{n_p \alpha_m} \quad (3.11)$$

where the difference in MMF over each segment can simply be written as

$$\Delta fq_k = fq_2 - fq_1 \quad (3.12)$$

$$\Delta fq_{h-1} = fq_h - fq_{h-1}, (h = 3, \dots, k) \quad (3.13)$$

$$\Delta fq_k = fq_{k+1} - fq_k. \quad (3.14)$$

As in the case with the iron segments, a quota between the average MMF and the air barriers size can be written as

$$\frac{W_h}{Wh + 1} = \left( \frac{\Delta fq_h}{\Delta fq_{h+1}} \right)^2 \quad (3.15)$$

There are however  $k$  unknown variables but only  $(k - 1)$  equations. By using the insulation ratio, the total length of the air barriers,  $l_a$ , can be calculated. Using the knowledge of,  $l_a$ , the length of each separate barrier can be calculated using the equations above. The total amount of air in the rotor,  $l_a$ , is easily calculated from the insulation ratio according to

$$l_a = \frac{\left( R_{rotor} - R_{shaft} \right)}{\left( 1 + \frac{1}{K_{wq}} \right)}. \quad (3.16)$$

It must be pointed out that this is a somewhat simplified version of the mathematical model described in [6]. The main difference is that this model only takes the q-axis widths into account. This is due to the fact that the air barriers and iron segments have the same width in both q and d-axis directions in this case. In the original model, the same design procedure as demonstrated above should be repeated, but this time for the d-axis. The insulation ratio and total length of iron available will ofcourse differ in d-axis direction compared from the q-axis direction.

## 3.2 Mathematical Model 2

The second mathematical model that will be used in this study is especially developed for this case and is somewhat similar to the first mathematical model. The purpose of this model is to demonstrate the impact of the segment and air barrier width with respect to the previous segment/air barrier. By introducing a new parameter  $jk$ , which is a chosen constant, the rate of growth for each segment is

determined. This model however needs to have the upper iron segment size pre-determined in order to work. If the total number of air barriers is  $k$ , then the total number of iron segments in the rotor will therefore be  $(k + 1)$ , given that the upper iron segment  $S_1$  is fixed. It is therefore recommended to sweep the size of the upper segment in combination with this mathematical model in order to find the most suitable combination for the specific application. The arrangement of the parameters are shown in detail in Fig. 3.2.

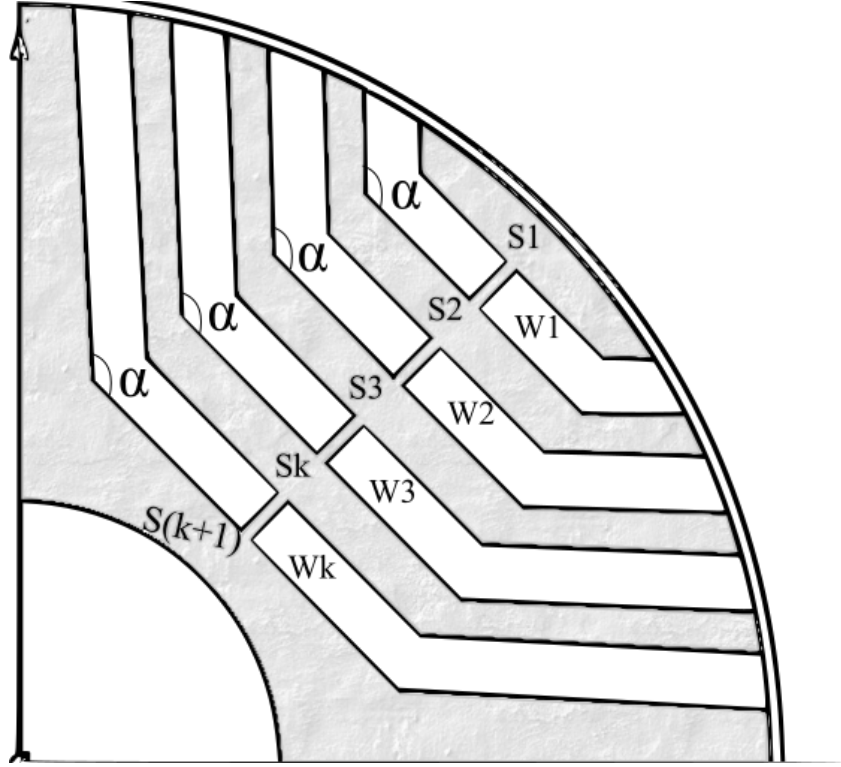


**Figure 3.2:** Position of the iron and air segment parameters for  $k$  air barriers and also the air barrier angle  $\alpha$

### 3.2.1 Segment Width

The total amount of iron in the rotor  $l_y$ , can as in the previous model be written as a sum of all iron segments such as

$$l_y = \sum_{h=1}^{k+1} S_h \quad (3.17)$$

where  $S_1$  is the top iron segment along the q-axis and should be fixed. With knowledge of both  $l_y$  and  $S_1$  the segment widths can be expressed as

$$(l_y - S_1) = \sum_{h=2}^{k+1} S_h \quad (3.18)$$

which gives only one equation but  $k$  unknown variables. Therefore the constant  $jk$

is introduced which shows the correlation between each iron segment. Each iron segment will grow with the factor  $jk$  compared to the previous segment. Thus can the length of each segment easily be calculated according to

$$(l_y - S_1) = S_h + S_h(jk)^{h-1} + S_h(jk)^h + S_h(jk)^{(h+1)} \dots, S_h(jk)^{(k-1)}, (h = 2) \quad (3.19)$$

$$S_h = \frac{(l_y - S_1)}{\left(1 + (jk)^{h-1} + (jk)^h + (jk)^{(h+1)} \dots, (jk)^{(k-1)}\right)}, (h = 2). \quad (3.20)$$

This means that the second iron segment from the top along the q-axis is given according to (3.20). The remaining segments for  $k$  number of air barriers can thereby be calculated as

$$S_3 = S_2(jk)^{(2-1)} \quad (3.21)$$

$$S_4 = S_2(jk)^2 \quad (3.22)$$

$$S_5 = S_2(jk)^{(2+1)} \quad (3.23)$$

⋮  
⋮  
⋮

$$S_{(k+1)} = S_2(jk)^{(k-1)}. \quad (3.24)$$

This leads to a flexibility when designing the rotor. By changing the design parameter  $jk$ , the growth rate of each segment is changed as well.

#### 3.2.2 Air barrier width

The methodology for calculating the air barrier widths is basically identical to the iron segment methodology. There are however some small differences. First and foremost, there is no need of pre-determination of a barrier width, unlike the case for iron segments. This results in that the width of the air barriers along the q-axis may be written as a function of the total amount of air in the rotor  $l_a$ . The total amount of air is given by the insulation ratio, as in previous cases. Using this and the constant,  $jk$ , the width of the air-barriers can be written as

$$l_a = W_h + W_h(jk)^h + W_h(jk)^{(h+1)} \dots, W_h(jk)^{(k-1)}, (h = 1) \quad (3.25)$$

$$W_h = \frac{l_a}{\left(1 + (jk)^h + (jk)^{(h+1)} \dots, (jk)^{(k-1)}\right)}, (h = 1). \quad (3.26)$$

The remaining air barriers for  $k$  number of barriers can now be determined according to following equations

$$W_2 = W_1(jk)^{(1+0)} \quad (3.27)$$

$$W_3 = W_1(jk)^{(1+1)} \quad (3.28)$$

·  
·  
·

$$W_k = W_1(jk)^{(k-1)} \quad (3.29)$$



# 4

## Case Setup

In order to produce a qualitative design of the rotor and evaluate the presented mathematical models, performing FEM analyses is essential. By making a model of the PMSM for FEM analyses, a reference is thereby produced for evaluating the performance of the SynRM. Before any FEM calculations can be performed by the simulation software, a proper simulation setup needs to be done. This chapter aims on providing the simulation setups in detail for both the SynRM and the PMSM.

### 4.1 Target Parameters

When performing simulations of different machines it is of importance to specify which parameters that are out of interest and should be evaluated. The parameters of main interest for this study are

- Average torque [Nm]
- Torque ripple [%]
- Power Losses [W]
- Saliency ratio

and based on these parameters the evaluation of the simulation results will be conducted and discussed.

### 4.2 Time steps and meshing

One very important aspect when performing any kind of simulations are the sampling frequency and the meshing of the model. For this thesis, the sampling frequency is directly dependent on the period time that is being simulated and the number of time steps. Therefore, it is wise to choose the parameters so that the period time becomes an even dividable number. This means that the last sample in the simulation will match the electrical period being simulated. In this study the simulations are being performed in steady state at different rotational speeds. This means that the simulation time,  $T_{stop}$ , and step time,  $T_{step}$ , can be calculated with knowledge of the electrical frequency. At a given rotational speed, in this case 4000 rpm, the electrical frequency can be written as

$$f_e = n_p * 4000/60 = 133.33[Hz] \quad (4.1)$$

and the length of one electrical period in seconds is

$$T_{per} = \frac{1}{f_e} = 7.5[ms] \quad (4.2)$$

Due to the iron losses and how they are being calculated, it is common practise to extract data from the second time period of the simulation. This means that the simulation duration time should be two electrical periods. Clearly,  $T_{stop}$ , can now be written as

$$T_{stop} = 2T_{per} = 15[ms] \quad (4.3)$$

and using 50 samples per period the step time can be calculated to

$$T_{step} = \frac{T_{stop}}{100} = 0.15[ms]. \quad (4.4)$$

With the time steps and simulation time sorted out, achieving good simulation performance does not only consist of choosing reasonable values defining these. Another important aspect is the meshing in the simulation model. Due to the physical properties of the SynRM, some areas of the motor will be less active than others. The geometry of the rotor will decide the size of the applied mesh for that specific area. The air gap will for instance require a finer mesh due to the frequent variations in this area. A large mesh will not be able to catch these variations. In a less active area, such as in the rotor near the shaft, the size of the mesh can be larger since it is not as sensitive to variations as the air gap. With the previously mentioned simulation times and with a mesh containing approximately 20 000 nodes, the total simulation time will be around 15 minutes. In Fig. 4.1, the mesh for different parts of the machine is illustrated. As can be seen, the mesh is refined around the air gap, while the coils and stator teeth have a larger mesh. Something which is of great importance in order to achieve good simulation results.

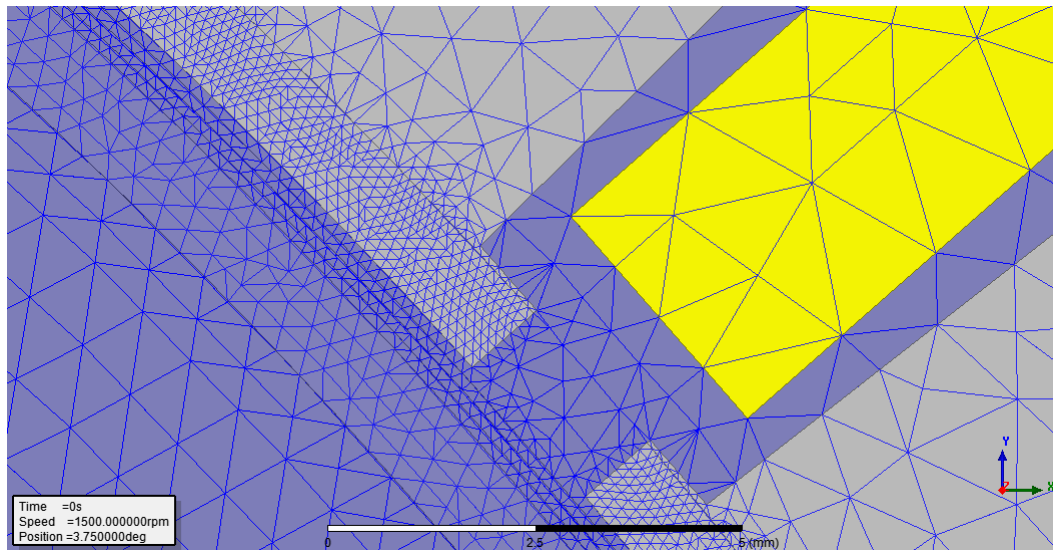


**Figure 4.1:** Mesh setup for the stator, air-gap and outer part of rotor

### 4.3 The SynRM Simulation Setup

In this study a 4-pole SynRM with a 48-slot stator is being analysed and will be compared with a 8-pole PMSM. This means that even if the stators are identical, the winding needs to be different to fit respective machine. The analyses of the machines are based on steady-state operation at different rotational speeds. In Table 4.1 below, some key data related to the initial simulation setup of the SynRM is presented.

SynRM Parameters	
Rotational speed	4000 $r/min$
Poles	4
Electrical frequency	133.33 $Hz$
Air gap	0.55 $mm$
Current Angle $\theta$	45°
Stator outer diameter	210 $mm$
Stator inner diameter	141.75 $mm$
Rotor diameter	140.65 $mm$
Active Length	150 $mm$
Barriers	4
Coil Area	25 $mm^2$
Parallel branches	2
Number of turns	4
Shaft diameter	48 $mm$
Stator slots	48

**Table 4.1:** SynRM simulation parameters

The stator of the SynRM has 48 slots, where each slot is containing a double layer winding. The total number of turns for each slot is  $N = 4$ . By letting the targeted maximum current density be  $J_v = 25 \text{ A/mm}^2$  the stator peak current can be calculated from the following equations [9]

$$S_{cu} = \frac{S_{coil}}{N} \quad (4.5)$$

resulting in a copper conductor area of  $6.25 \text{ mm}^2$ . This means that with two parallel branches, each of the branches carries half of the stator current. Then, by using the current density equation the peak stator current is calculated according to

$$I_{s,peak} = 2(J_v S_{cu}) \quad (4.6)$$

resulting in a peak current of  $I_{s,peak} = 312.5 \text{ A}$ . With the knowledge of the peak phase current, the three phase currents can now be expressed as

$$I_{s,A} = I_{s,peak} \cos(\omega_r t + \phi) \quad (4.7)$$

$$I_{s,B} = I_{s,peak} \cos(\omega_r t + \phi - \frac{2\pi}{3}) \quad (4.8)$$

$$I_{s,C} = I_{s,peak} \cos(\omega_r t + \phi + \frac{2\pi}{3}). \quad (4.9)$$

Since the SynRM is operated in the d-q reference frame the alignment of the d and q-axes are out of importance. One alternative is where the direct axis should be aligned with the positive A-phase flux at  $t = 0$ [1]. In a 4-pole SynRM at  $t = 0$  the q-axis is therefore directed directly into the  $A^+$  phase according to Fig. 4.2, below. The figure also demonstrates the barrier sweep angle  $\alpha$ , which is the angle that will be swept in forthcoming simulations.

It should be noted that the barrier sweep angle  $\alpha$  should not be mixed with the stator slot pitch angle  $\alpha_m$  from Mathematical Model 1.

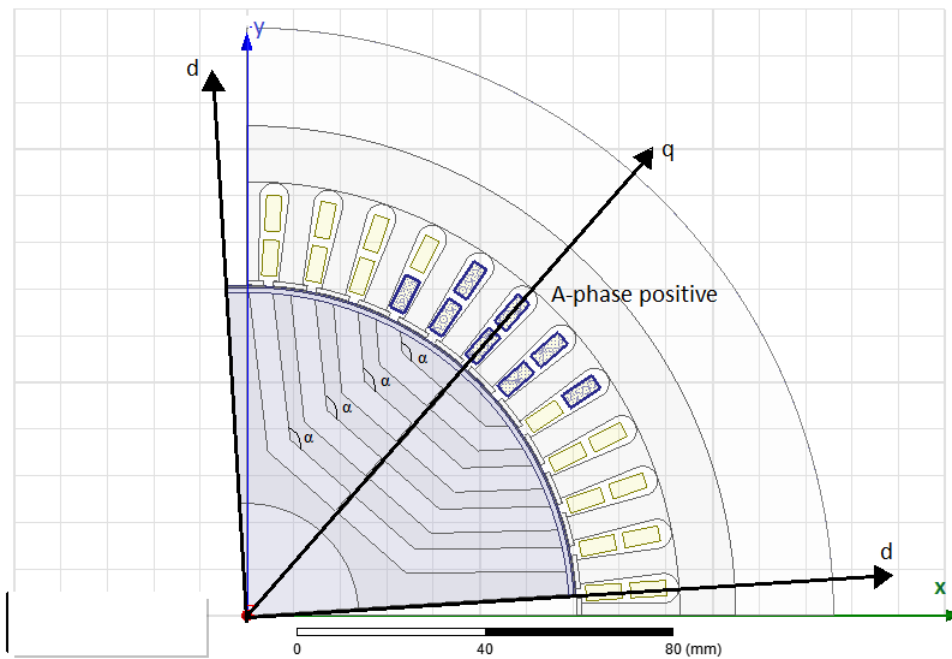


**Figure 4.2:** SynRM d-q axis setup at  $t = 0$  and barrier sweep angle  $\alpha$

## 4.4 The PMSM Simulation setup

For this study, a PM reference motor is provided. Due to its nature as a reference motor, all the parameters are fixed. The only variable that will change for the PMSM speed at which it is rotating. In Table 4.2, some of the initial simulation key parameters are demonstrated for the PMSM.

The 8-pole PMSM machine is operated at a peak current of  $420\text{ A}$  and with 4 parallel branches and 6 number of turns for each coil. The total area of the coils are identical to the one in the SynRM. Using (4.5) and (4.6), the current density is calculated to  $Jv = 25.5\text{ A/mm}^2$  which is almost identical to the current density in the SynRM. The phase currents in the PMSM can be expressed identically to the ones in the SynRM, written as

$$I_{s,A} = I_{s,peak} \cos(\omega_r t + \phi) \quad (4.10)$$

$$I_{s,B} = I_{s,peak} \cos(\omega_r t + \phi - \frac{2\pi}{3}) \quad (4.11)$$

$$I_{s,C} = I_{s,peak} \cos(\omega_r t + \phi + \frac{2\pi}{3}) \quad (4.12)$$

One difference in the PMSM compared to the SynRM is the alignment of the d and q-axis. This means that for an PMSM the flux will go in the direction of what is

PMSM Parameters	
Rotational speed	4000 <i>r/min</i>
Poles	8
Electrical frequency	266.66 <i>Hz</i>
Air gap	1.575 <i>mm</i>
Current Angle $\theta$	135°
Stator outer diameter	210 <i>mm</i>
Stator inner diameter	141.75 <i>mm</i>
Rotor diameter	140.175 <i>mm</i>
Active Length	150 <i>mm</i>
Coil Area	25 <i>mm</i> <sup>2</sup>
Parallel branches	4
Number of turns	6
Shaft diameter	84 <i>mm</i>
Stator slots	48

**Table 4.2:** PMSM simulation parameters

the q-axis in the SynRM. This means that for a PMSM, the d-axis is aligned in the center of the pole while the q-axes are at the edge of the poles [1]. The alignment of the d-q axes in the PMSM can be seen in Figure 4.3.



**Figure 4.3:** PMSM d-q axis setup at  $t = 0$

# 5

## Analysis

With the different mathematical models and a proper simulation setup, the simulations can be performed. The core of this study is to compare the reference PMSM with a suggested design for the SynRM. Before any final design can be suggested for the SynRM, the machine designs produced by the mathematical models need to be evaluated. To do this, a step by step procedure is needed. Due to the many variables that affect the performance of the system, it is essential to sweep a limited number of variables each simulation run in order to be able to find which variable that affects the performance. When enough data is collected, the aim is to choose the best performing design of the SynRM and compare it to the reference PMSM. The aim of this chapter is to provide simulation results and an analysis of these result, which will be a basis for the final conclusions.

### 5.1 The SynRM Initial Model

The first step towards finding a suitable rotor design is to realize the mathematical models presented earlier, in order to evaluate different designs. Even with the help of the mathematical models which should provide a sufficient design, trial and verification of these is still needed. By introducing an initial model, a basis for the first simulations is created and so is the first step towards finding the final design of the SynRM rotor.

#### 5.1.1 Mathematical Model 2 - S1 Selection

The initial simulations are performed to study the impact of the first iron segment length  $S1$  on the impact on the machine. For this case, the Mathematical model 2 is used with a fixed insulation ratio of ( $K_{wq} = 0.5$ ) and the constant ( $jk = 1.2$ ) to model the rotor. Other values than these can be used, since the MM2 does not provide any specific rule for the selection of these. The lengths of  $S1$  that are evaluated stretches from 3 mm to 6 mm, since for values lower than 3 mm the top air barrier comes to close to the rotor edge in q-axis direction. The maximum value of 6 mm is chosen because for values higher than 6 mm for  $S1$ , the air barriers given by MM2 ends up outside the pole for certain low and high angles of  $\alpha$ . The rest of the simulation parameters are fixed according to the simulation setup described in Section 4.3. By using these parameters, data have been extracted from the simulation results and Fig. 5.1 and 5.2 are showing the torque performance. In Fig. 5.3 the iron losses,  $P_i$  can be seen. This is due to that the copper losses,  $P_{cu}$ , will be

the same for all values of  $S1$ , since the machine is operated at the same point for all the cases. The copper losses are extracted from the simulations are,  $P_{cu} = 2472 W$ . Note that each value in the graphs represent an average value over the simulation time for that specific setup.

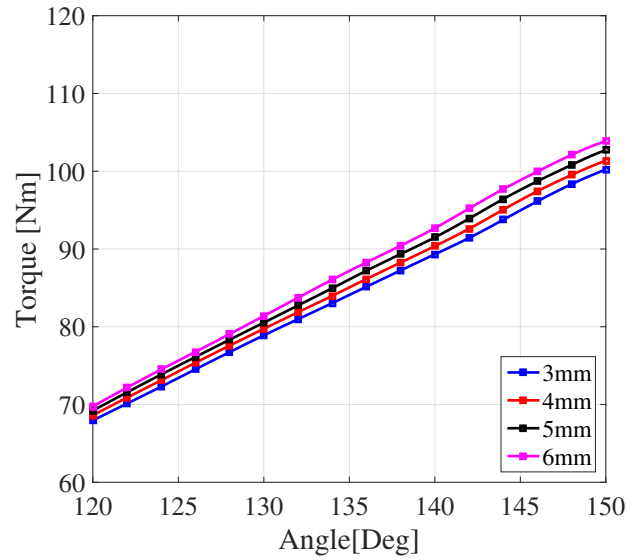


**Figure 5.1:** Average torque for different  $S1$ ,  $Kwq=0.5$ ,  $jk=1.2$ , 4000 r/min

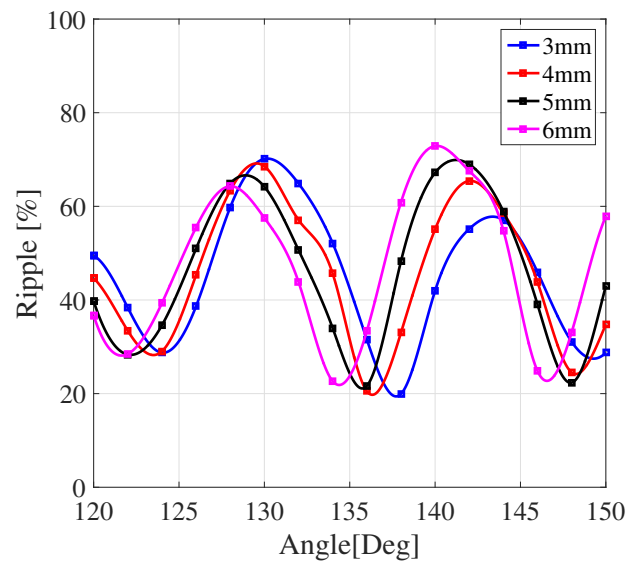


**Figure 5.2:** Torque ripple for different  $S1$ ,  $Kwq=0.5$ ,  $jk=1.2$ , 4000 r/min

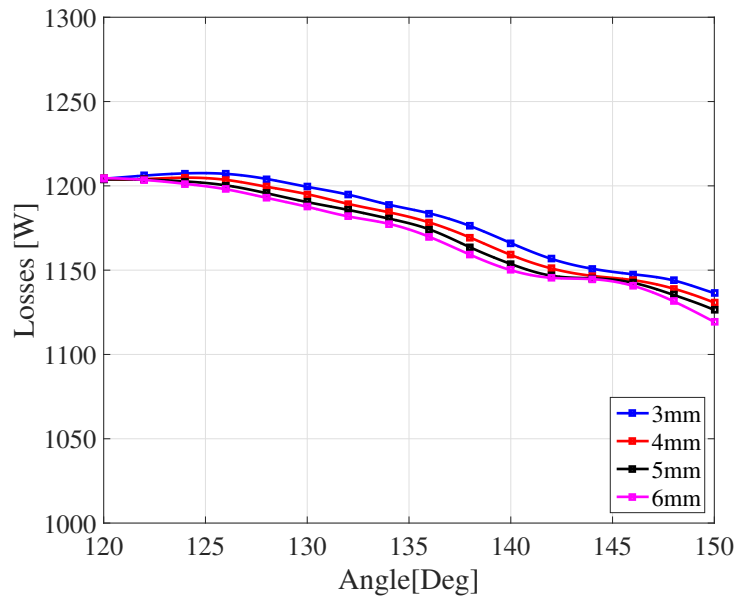


**Figure 5.3:** Iron losses for different S1,  $K_{wq}=0.5$ ,  $j_k=1.2$ , 4000 r/min

#### 5.1.1.1 S1 selection - Analysis

At this stage of the process, the main task is to determine the length of the top iron segment S1. From Fig. 5.1 and 5.2, data can be extracted which shows that the highest average torque is achieved for  $S1 = 6 \text{ mm}$ . The torque ripple is however a bit higher for 6 mm compared to the other values. The effect that increasing the length of S1 have on the ripple is that the amplitude of the ripple increases. It can also be seen from Fig. 5.2 that the ripple depends on how the air barriers match the stator slots. This is an indication that the ripple is highly dependent on the angle of the air barriers. This is further evaluated in Section 5.2. The peak-to-peak values on the ripple will increase for higher values on S1, which means that for certain angles the ripple may be extremely high, but for others low. For now at this stage, the ripple is of less importance since the ripple optimisation will occur at a later stage. The losses also decrease when the S1 iron segment is increased, and they also decrease with a higher angle. This may be because higher angle for the air barriers means that the d-axis flux will have an more direct path thought the rotor. This means that there will be less saturation and the iron losses will decrease. Therefore,  $S1 = 6 \text{ mm}$  is the value that will be used for S1 in forthcoming simulations.

### 5.1.2 Model Comparison - Torque Performance

With the  $S1$  decided from previous simulations, the Mathematical Model 2 now have a fixed value for  $S1$ . This means that a comparison between the different mathematical models can now be done for different insulation ratios and different modeling constants  $jk$ . As in the previous case, a sweep is done over the barrier angle  $\alpha$  in order to demonstrate the relation between  $\alpha$  and changes in performance.

The main idea is to compare the designs given by Mathematical Model 1 (MM1) and Mathematical Model 2 (MM2) for different insulation ratios stretching from 0.5 – 0.9. Each insulation ratio results in a specific design, which is evaluated for every air barrier angle  $\alpha$ . For the torque performance, the average torque and the average torque ripple is studied in presented. Since the MM2 was developed specifically for comparison with MM1, a similar procedure is used for MM2 as for MM1. However, since MM2 uses slightly different parameters than MM1, the MM2 will produce three different model, each model having a different modeling constant,  $jk$ . Three different modeling constants are chosen for this study,  $jk = 1$ ,  $jk = 1.2$ , and,  $jk = 1.4$ , which should provide noticeable differences in the designs. All of these are evaluated for insulation ratios between 0.5 – 0.9, just as MM1 in order to provide a fair comparison. The total number of models is therefore four (one variant for MM1 and three variants for MM2).

Some modeling parameters will allow a higher  $\alpha$  than others, which means that for some models there will be more data available than for others due to the different physical constraints. A thorough analysis for all four models is done later on in the analysis section of the model comparison.

In theory, the average torque should increase with an higher insulation ratio, since more air in the rotor will help to reduce the q-axis flux while letting the d-axis flux remain the same. However, to much air in the rotor will start to reduce the d-axis flux and therefore, the insulation ratio can not be to high. A larger air barrier angle  $\alpha$  means that the shape of the air barriers will be similar to the flux lines in the rotor, thus allowing an smoother passage of these thought the iron. However, if the air barrier becomes to large, tha air barriers will not fit in the pole. Therefore, there is a limit on how much the average torque can increase. For MM1, these effects can be seen in Fig. 5.4 and 5.5.

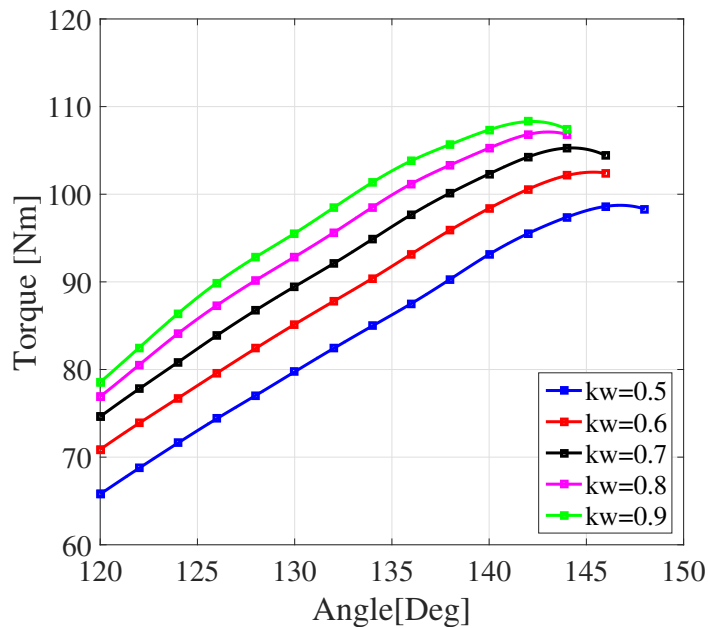


**Figure 5.4:** Average Torque in MM1 for different Kwq, 4000 r/min

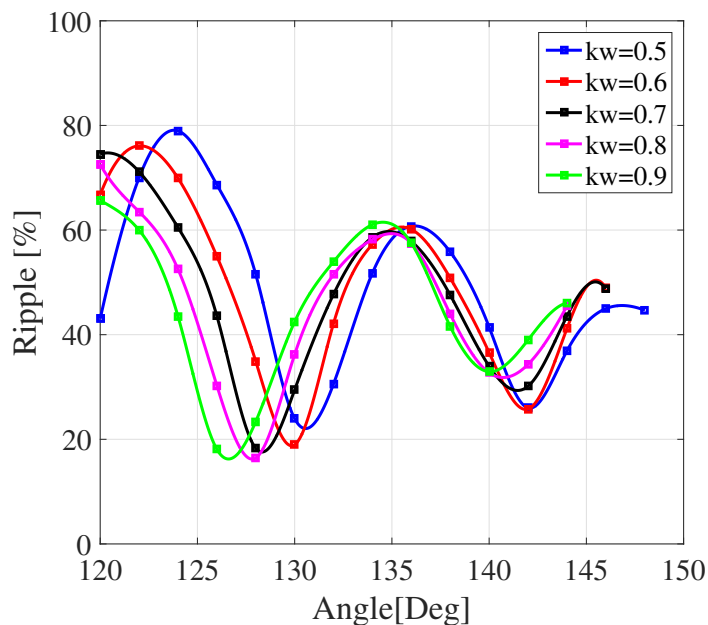


**Figure 5.5:** Average Torque Ripple in MM1 for different Kwq, 4000 r/min

The behaviour of the torque and the torque ripple for MM2 is similar to those in MM1 but, for MM2 the modeling parameter  $jk$  will play an important role. Since  $jk$  controls the amount of air in each barrier, related to the insulation ratio, there will be difference mainly in the ripple maximum and minimum values. Most of the flux passes through the lowest two iron segments, which means that if the lowest air barrier is large, the difference in ripple for an increased air barrier angle will not

be as significant for a low  $jk$  as for an higher value of  $jk$ . This can be seen clearly in the six figures presented below. In Fig. 5.6 and 5.7 the torque characteristics for  $jk = 1$  are displayed, Fig. 5.8 and 5.9 show characteristics for  $jk = 1.2$  and finally the data for  $jk = 1.4$  can be found in Fig. 5.10 and 5.11.

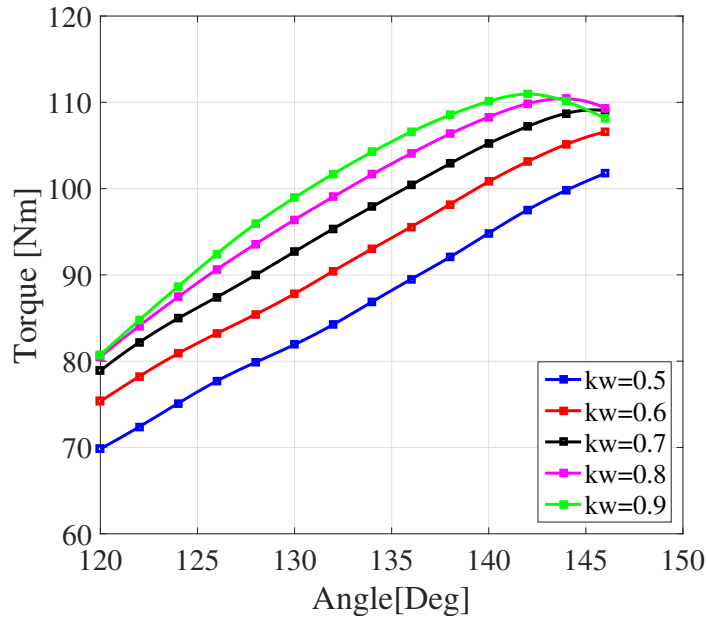


**Figure 5.6:** Average Torque in MM2 for different Kwq,  $jk=1.0$ , 4000 r/min

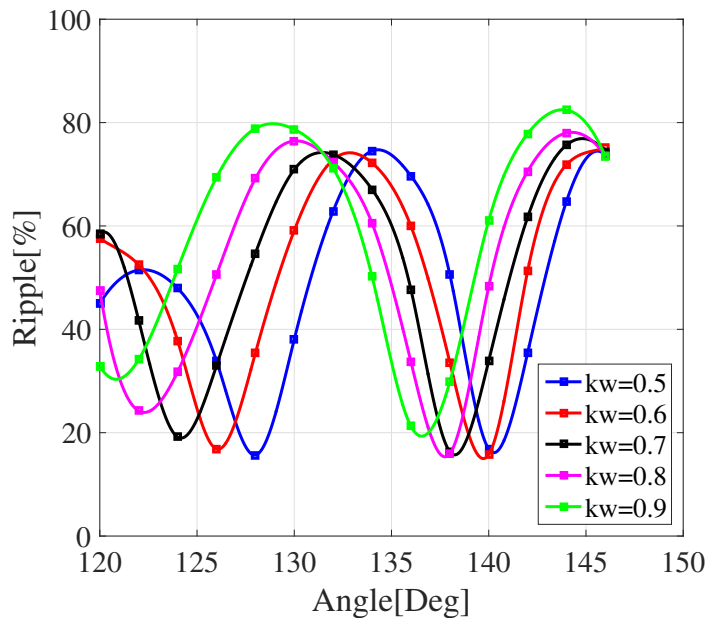


**Figure 5.7:** Average Torque Ripple in MM2 for different Kwq,  $jk=1.0$ , 4000 r/min

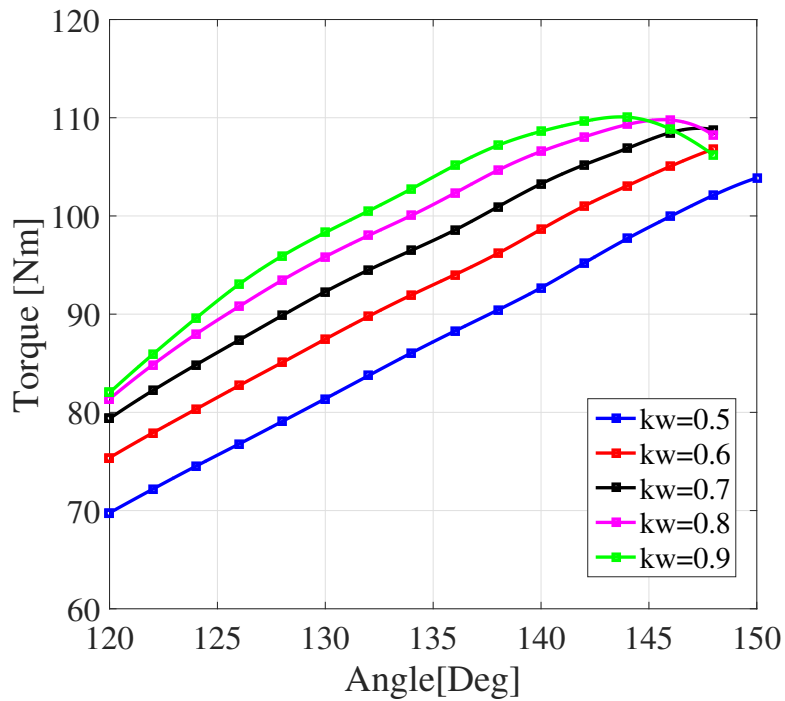


**Figure 5.8:** Average Torque in MM2 for different Kwq,  $jk=1.2$ , 4000 r/min

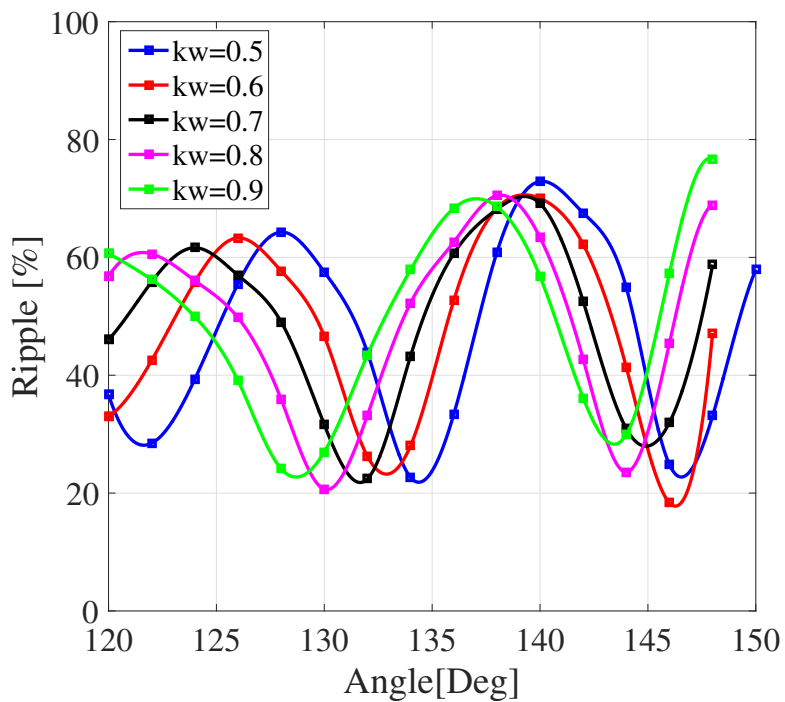


**Figure 5.9:** Average Torque Ripple in MM2 for different Kwq,  $jk=1.2$ , 4000 r/min

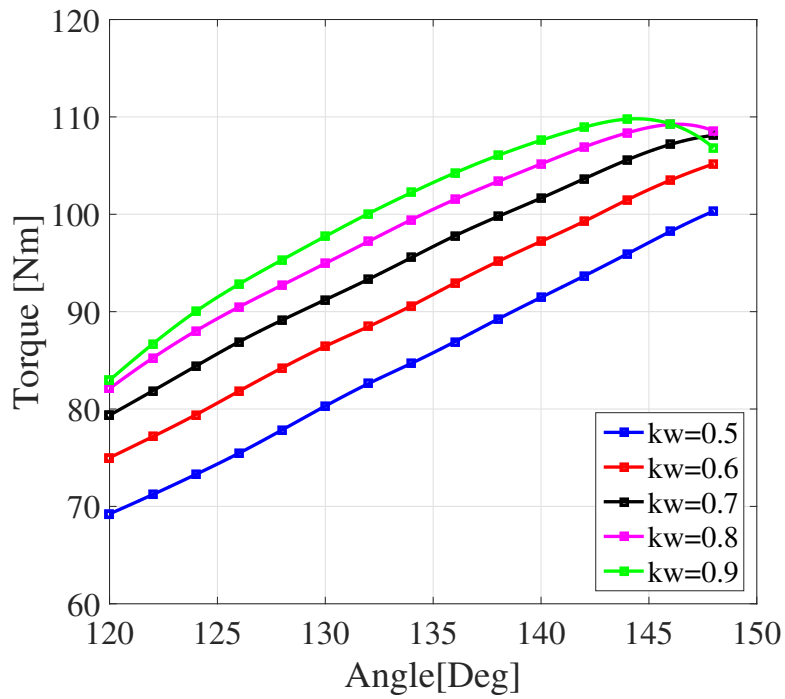


**Figure 5.10:** Average Torque in MM2 for different Kwq, jk=1.4, 4000 r/min

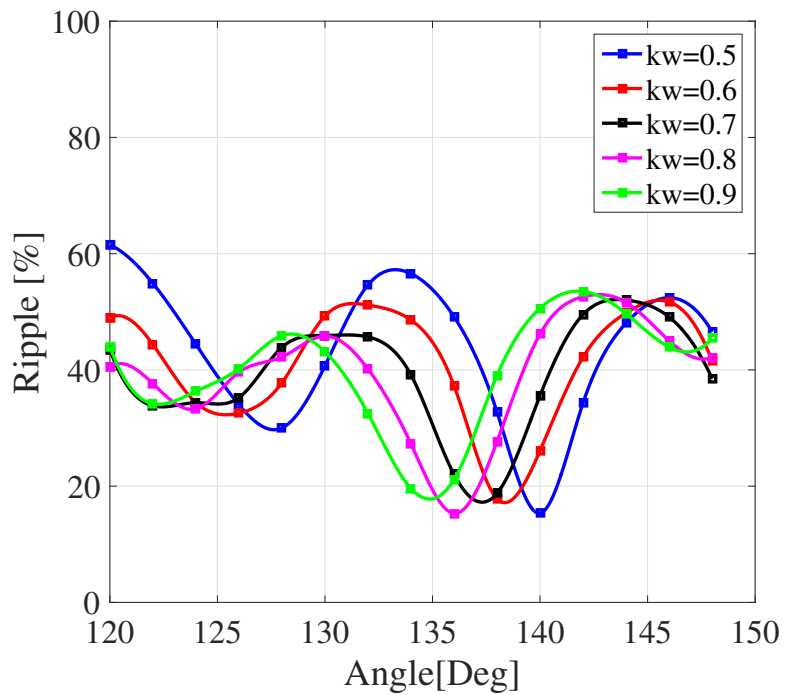


**Figure 5.11:** Average Torque Ripple in MM2 for different Kwq, jk=1.4, 4000 r/min

### 5.1.3 Model Comparison - Losses

One other important aspect in the the overall performance is the losses. In this case, the losses presented below are the iron losses for each design and insulation ratio. Since the machine is still operated at the same point of operation as in previous simulations, the restive losses,  $P_{cu}$ , are still 2472 W. By increasing  $\alpha$ , the iron losses should be reduced due to the more natural flux path achieved by the increase of  $\alpha$ . Due to the even distribution of the air barriers in MM2 for  $jk = 1$ , ande somewhat in MM1, the iron losses are expected to be lower in these than in the rest of the MM2 designs. However, the impact should not be major, but small differences can be expected. The iron losses for MM1 can be seen in Fig. 5.12 and for MM2,  $jk = 1$ , in Fig. 5.13.

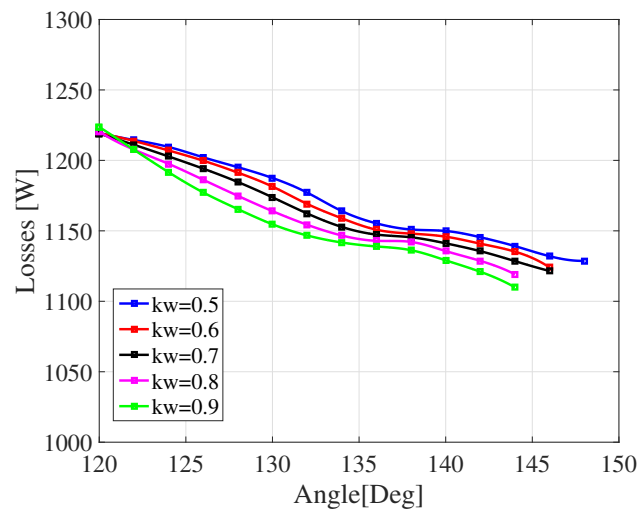


**Figure 5.12:** Iron losses in MM1 for different Kwq, 4000 r/min

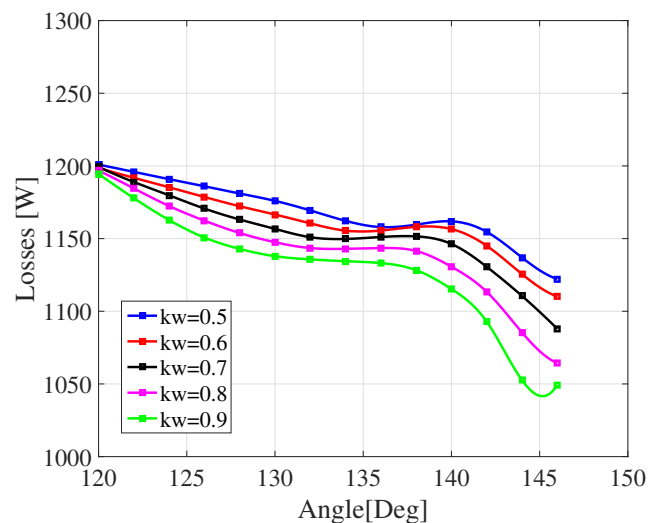


**Figure 5.13:** Iron losses in MM2 for different Kwq,  $jk=1.0$ , 4000 r/min

The iron losses for MM2 where  $jk = 1.2$  and  $jk = 1.4$  can be demonstrated below in Fig. 5.14 and 5.15. As expected, they are somewhat higher than for the previous two. When the resistive losses are added, this small increase in iron losses will not affect the overall efficiency of the machine.

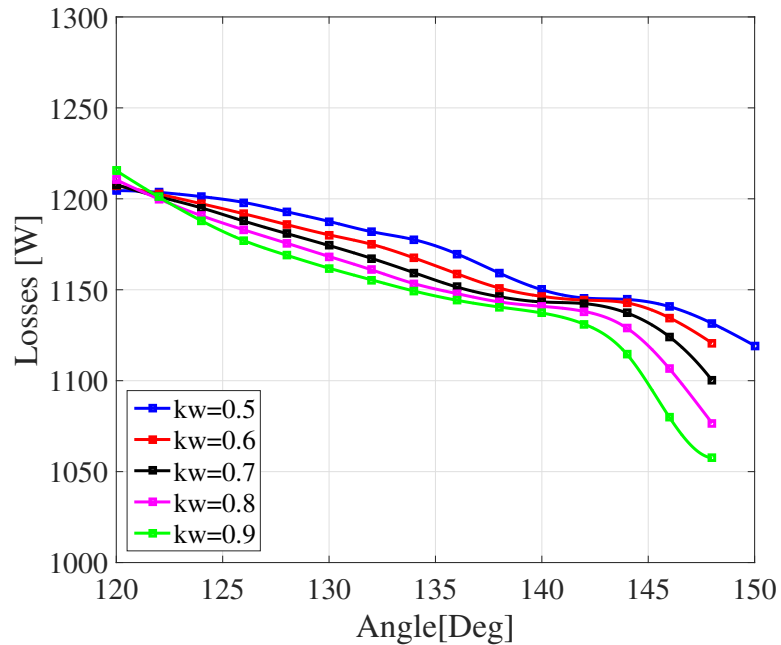


**Figure 5.14:** Iron losses in MM2 for different Kwq,  $jk=1.2$ , 4000 r/min

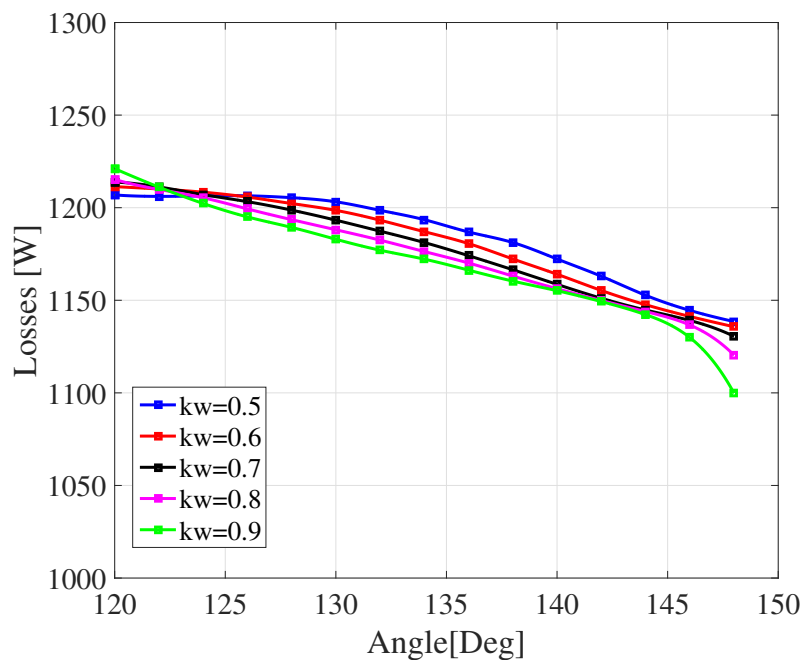


**Figure 5.15:** Iron losses in MM2 for different Kwq,  $jk=1.4$ , 4000 r/min

### 5.1.4 Model Comparison - Saliency Ratio & Efficiency

As mentioned, one key parameter for performance indication is the saliency ratio and the efficiency of the machine. For this simulation case, a low saliency ratio could be expected. As shown in the simulation setup section, the simulations were performed on maximum current and an, in theory, optimal current angle. This will lead to saturation in d-axis direction, thus minimizing  $L_d$  and reducing the saliency ratio. The efficiency is calculated according to (2.35) in Chapter 2. In Fig. 5.16 and 5.17 the saliency ratio and efficiency for MM1 are demonstrated.

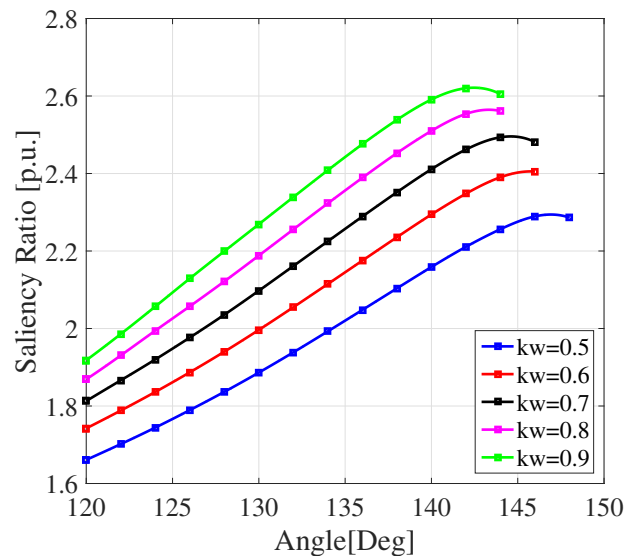


Figure 5.16: Saliency ratio in MM1 for different  $K_{wq}$ , 4000 r/min

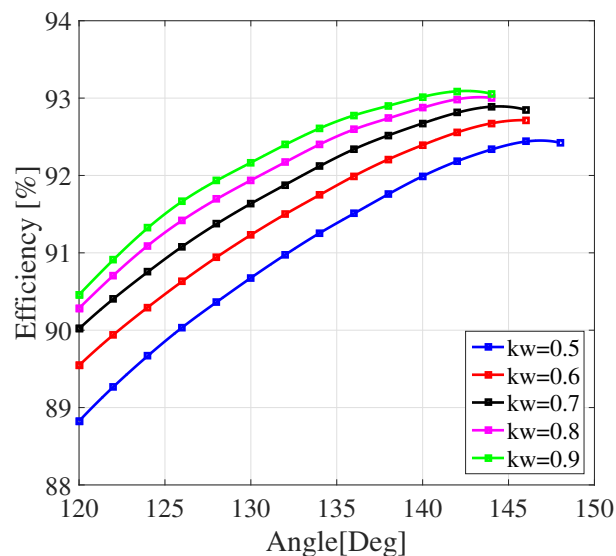
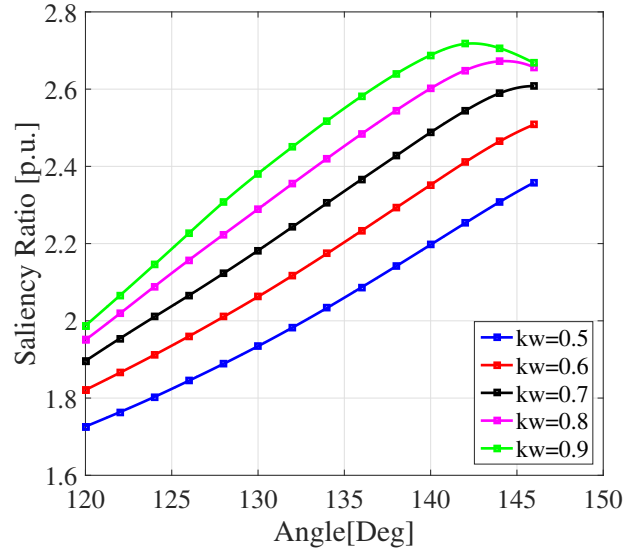
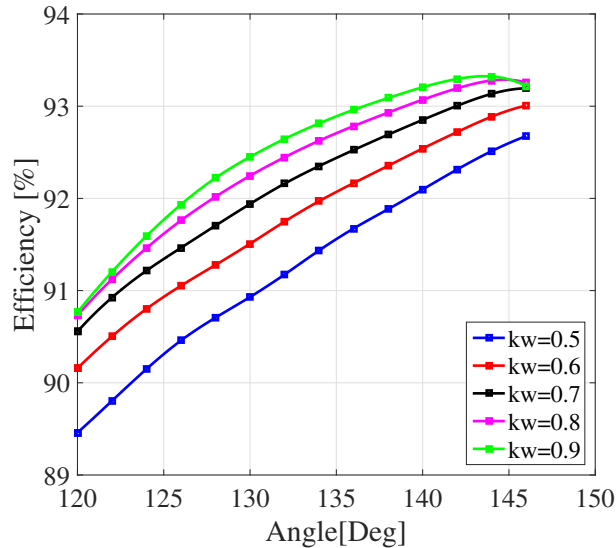


Figure 5.17: Efficiency in MM1 for different  $K_{wq}$ , 4000 r/min

The difference in saliency ratio between MM1 and MM2 is small. This an indication that the rotor is saturated at this point of operation. It can also be seen that the differences in iron losses does not affect the overall efficiency of the machine since the copper losses are higher than the iron losses. In Fig. 5.18 and 5.19 the saliency ratio and efficiency for MM2,  $jk = 1$ , are demonstrated.



**Figure 5.18:** Saliency ratio in MM2 for different Kwq,  $jk=1$ , 4000 r/min



**Figure 5.19:** Efficiency in MM2 for different Kwq,  $jk=1$ , 4000 r/min

The efficiency is somewhat lower in MM2,  $jk = 1.2$  compared to the design where  $jk = 1$ . This is due to the the difference in iron losses is rather small and therefore does not change the efficiency a lot. In Fig. 5.20 and 5.21 the saliency ratio and efficiency for MM2,  $jk = 1.2$  are displayed.

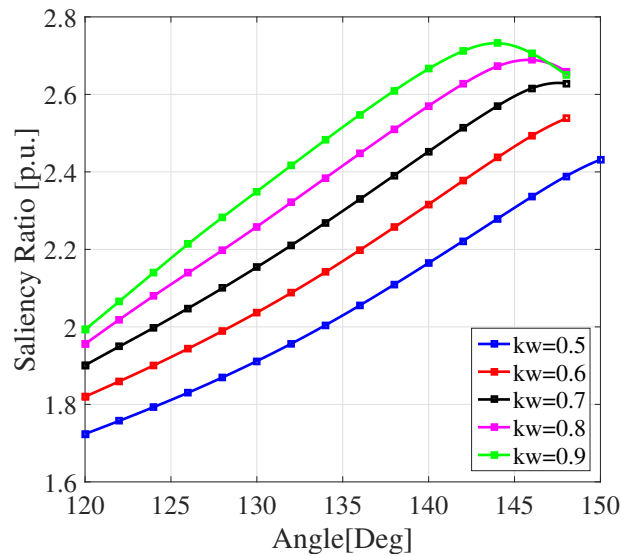


**Figure 5.20:** Saliency ratio in MM2 for different Kwq,  $jk=1.2$ , 4000 r/min

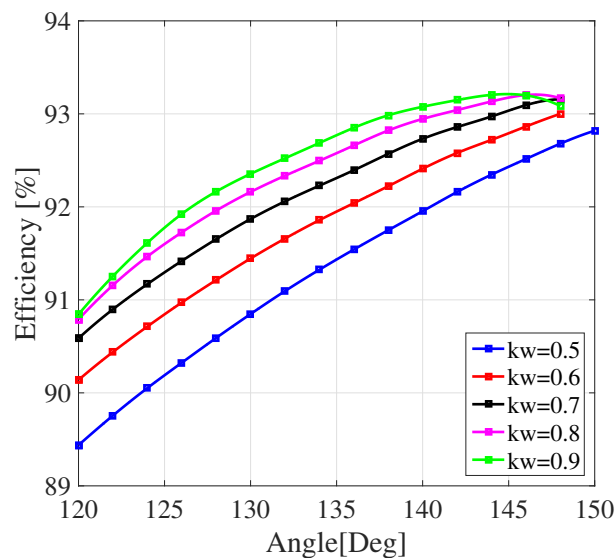


**Figure 5.21:** Efficiency in MM2 for different Kwq,  $jk=1.2$ , 4000 r/min

Finally, Fig. 5.22 and 5.23 shows the saliency ratio and efficiency for MM2,  $jk = 1.4$ .

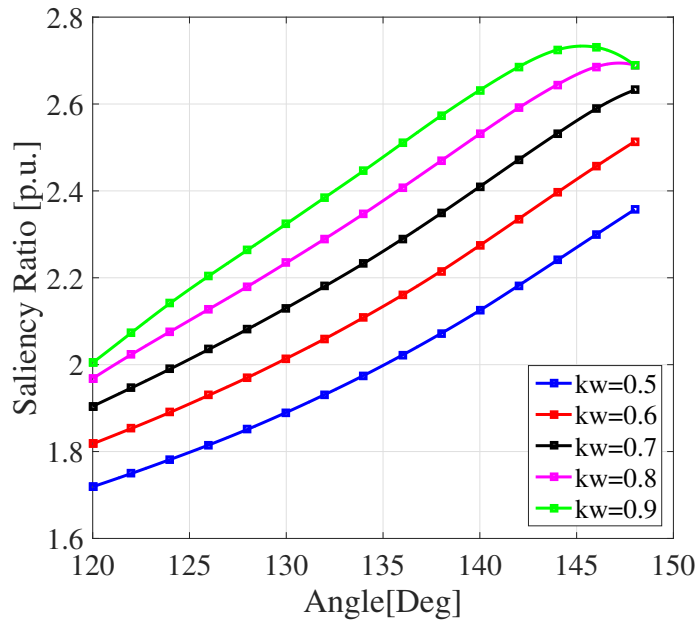


Figure 5.22: Saliency ratio in MM2 for different Kwq,  $jk=1.4$

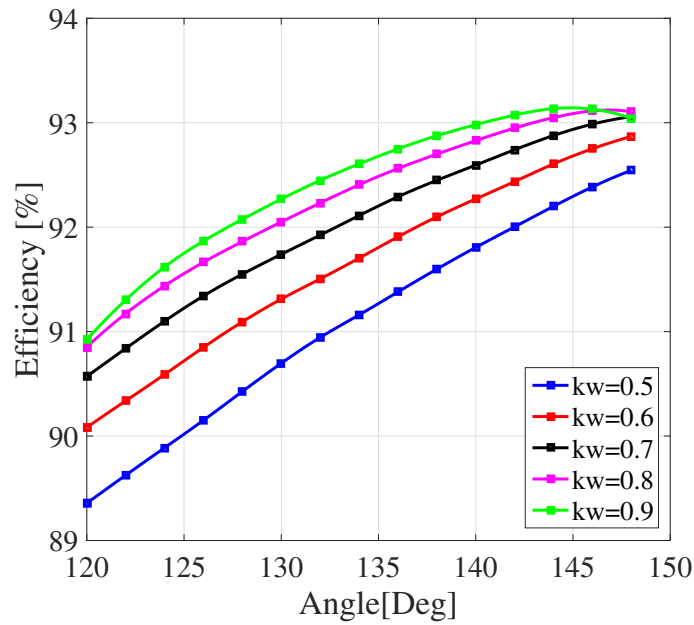


Figure 5.23: Efficiency in MM2 for different Kwq,  $jk=1.4$

### 5.1.5 Model Comparison - Analysis

Initially, it should be said, that all four models shows that performance for barrier angles  $\alpha$  below  $130^\circ$  are not sufficient. A low barrier angle  $\alpha$  means that the path of the flux lines is disturbed in such a way that the average torque cannot perform well. This means that the points of interest lies above this angle. One effect that can be seen is that the amplitude of the torque ripple curves is decreased when the air barrier width is decreased for the top barriers. More specific, when the rotor design is calculated according to MM1 and for high  $jk$  in MM2. The lowest values for the torque ripple and the highest average torque value is achieved when  $jk = 1$  in MM2. This design outperforms the other in this aspect. It should, however, be noticed that the difference in performance is considered small.

The losses decreases in this case compared to the others whilst the saliency ratio and efficiency is basically constant. The low saliency ratio can be related to saturation in the machine. This is an indication that the currents are too high or that the current angle is not optimal. This will be analysed more in detail in forthcoming chapters. Since the q-axis flux is low in the air barriers near the air gap, the outer air barriers may be thinner, thus leaving more space for the magnetic flux to travel in the iron. This will have an overall small effect on the complete system. Most of the flux passes through the lower iron segments and therefore leads to a smaller impact on the system compared to the top air barriers. By looking on MM2 for  $jk = 1$  and  $jk = 1.4$ , with an insulation ratio of 0.8, only small differences can be seen in the torque performance, demonstrated in Fig. 5.5 and 5.7. The impact of the insulation ratio is also major. In general, an increase in air in the rotor will reduce the q-axis inductance,  $L_q$  which will improve the performance of the machine. The key is to not reduce too much of the iron, thereby trying to prevent saturation and a drop in d-axis inductance. An indication that this effect is occurring is that for MM2  $jk = 1$  the ripple begins to increase again for  $K_{wq} = 0.9$  compared to  $K_{wq} = 0.8$ , while the peak torque sees an insignificant increase, as can be seen in Fig. 5.5 and 5.9. Since this study is limited in both time and coverage, a choice was made to only look at insulation ratios below 1. This means that to broaden the spectrum, it would be convenient to also analyse insulation ratios higher than 1. This, in order to confirm the indication that the performance will start to drop for high insulation ratios.

It should be pointed out that the results from the simulations are very similar and overall close to each other. No model outperforms the others. Also, the MM1 have been slightly modified in this thesis compared to the original. In this study, MM1 only considers the q-axis direction when calculating the widths of the barriers. In the original model, the air barriers should have a different width in d-axis direction. A separate study could be an option to further evaluate MM1, but these results indicates that even if improvement can be made, it is a matter of a few newton-meters in average torque and a few percent in ripple. This applies to the other tested model as well. There is no major difference between the models, and even if improvements are made, the hypothesis is that it is a matter of small numbers. With this in mind, it is still interesting to study the impact of the barriers position towards the stator slots. For doing this, a model needs to be selected. Due to good

average torque, relatively low losses and low ripple, the model produced by MM2 with  $jk = 1$  and  $Kwq = 0.8$  are used in forthcoming analysis to see if there is any possibilities of improvement of the overall performance. Even if some of the results indicates that there can be better performing setups, this one is a convenient layout for forthcoming analysis.

## 5.2 SynRM Asymmetric Ripple Reduction

So far, the design of the rotor have been symmetric in that sense that the air barrier angle  $\alpha$  have been the same for each barrier. By choosing a suitable case with high performance from the simulations above, the next step is to study the impact each barrier have on the overall performance of the machine. More specific, by using an asymmetric design of the rotor, it becomes possible to control the air barrier positions towards the stator individually. This may lead to some improvement in the performance of the machine. By determining the bottom barrier with data used from previous simulations, the angle  $\alpha$  for the remaining barriers can be expressed as

$$\begin{aligned}\alpha_1 &= Sweep \\ \alpha_2 &= \frac{\alpha_4 - \alpha_1}{3} + \alpha_1 \\ \alpha_3 &= 2\left(\frac{\alpha_4 - \alpha_1}{3}\right) + \alpha_1 \\ \alpha_4 &= 138^\circ\end{aligned}\tag{5.1}$$

which means that by changing the angle of the top barrier, the two remaining will automatically follow. Here,  $\alpha_1$  is the top air barrier and  $\alpha_4$  is the bottom air barrier. With this setup, several different asymmetrical designs can be tested with the change of only one parameter. The setup can be divided into three different cases where Case 1 is

$$\begin{aligned}\alpha_1 &= Sweep \\ \alpha_2 &= \alpha_4 \\ \alpha_3 &= \alpha_4 \\ \alpha_4 &= 138^\circ\end{aligned}\tag{5.2}$$

and Case 2 can be written as

$$\begin{aligned}\alpha_1 &= Sweep \\ \alpha_2 &= \frac{\alpha_4 - \alpha_1}{3} + \alpha_1 \\ \alpha_3 &= \alpha_4 \\ \alpha_4 &= 138^\circ\end{aligned}\tag{5.3}$$

and finally Case 3 is given from the following expression

$$\begin{aligned}
 \alpha_1 &= Sweep \\
 \alpha_2 &= \frac{\alpha_4 - \alpha_1}{3} + \alpha_1 \\
 \alpha_3 &= 2\left(\frac{\alpha_4 - \alpha_1}{3}\right) + \alpha_1 \\
 \alpha_4 &= 138^\circ.
 \end{aligned} \tag{5.4}$$

By using these cases, several different asymmetric designs can be evaluated.

### 5.2.1 Asymmetric Design - Analysis

As in previous cases, the same output data is studied in order to evaluate the performance of the machine. Initially, the torque characteristics of the asymmetric model is presented in Fig. 5.24 and 5.25.

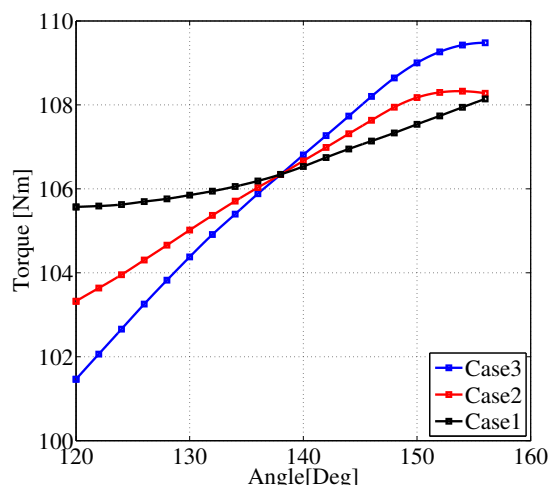


**Figure 5.24:** Average Torque in asymmetric model for different cases

It becomes evident that the ripple can be lowered even further at a very low cost in average torque. In Fig. 5.25, both Case 2 and Case 3 show significant improvement in torque ripple compared to the previous design suggestion. Small changes in the angle  $\alpha$  can result in rapid changes in torque ripple. These results also indicate that the top barrier alone has insignificant effect on the overall performance, which seems reasonable, since most of the flux is passing through the lower iron segments. By studying Fig. 5.24 and 5.25 in further detail, for Case 3,  $\alpha_4 = 138^\circ$  and  $\alpha_1 = 136^\circ$  the torque ripple is reduced to approximately 11% whilst the losses in average torque are minimal. In Fig. 5.26 the final design which produces these results is displayed. It can be seen that the air barriers are almost perfectly aligned with the stator slots. Due to the width of the air barriers combined with the barrier angle, each barrier basically cover the whole stator slot and some part of the stator tooth. This means that for any small changes in rotor position, the changes in  $L_d - L_q$  will not be drastic, thus will the torque not differentiate greatly over short time. The

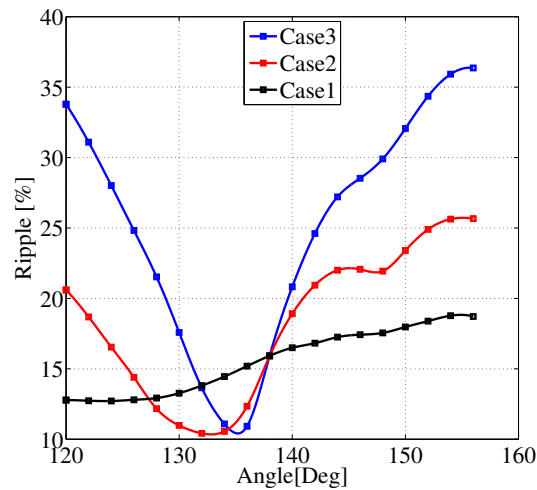


**Figure 5.25:** Torque ripple in asymmetric model for different cases

main reason for this behaviour is that, if the air barriers in the rotor is perfectly aligned with the stator slots and the stator teeth, the flux transfer will be optimal. If this position offsets slightly, the flux transfer between the stator and rotor will not be optimal and will therefore drop. This means that the torque will drop for a small change in rotor position, as mentioned. What follows is a high torque ripple. However, if the air barriers are slightly wider and overlap the stator teeth, the peak torque will not be as high, since it is not the optimal position, but the ripple won't be as high either. Any changes in rotor position will not produce large differences in peak torque and therefore, the ripple is reduced. In Fig. 5.27 and 5.28 below, the saliency ratio and efficiency for the asymmetric design is showed.

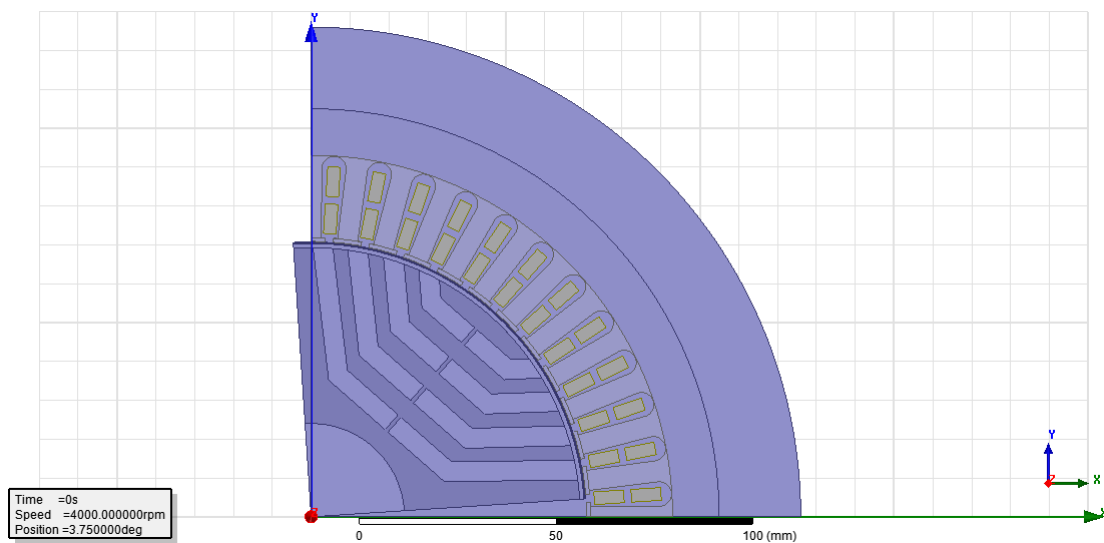


**Figure 5.26:** Assymmetric design of the SynRM rotor for  $\alpha_1 = 136^\circ$  and  $\alpha_4 = 138^\circ$

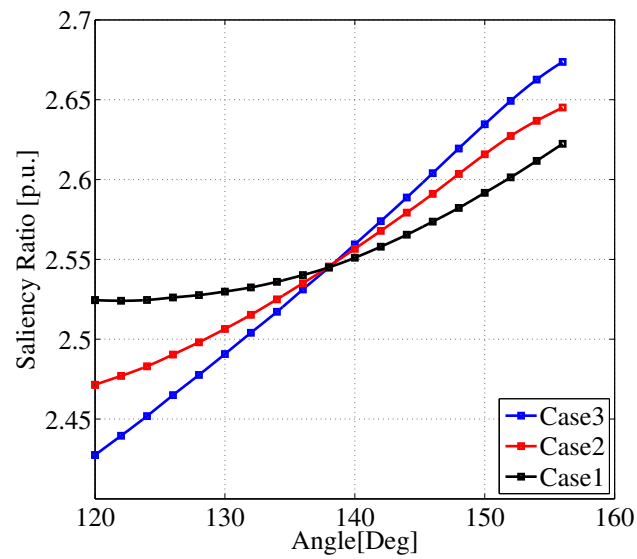


**Figure 5.27:** Saliency ratio in asymmetric model for different cases

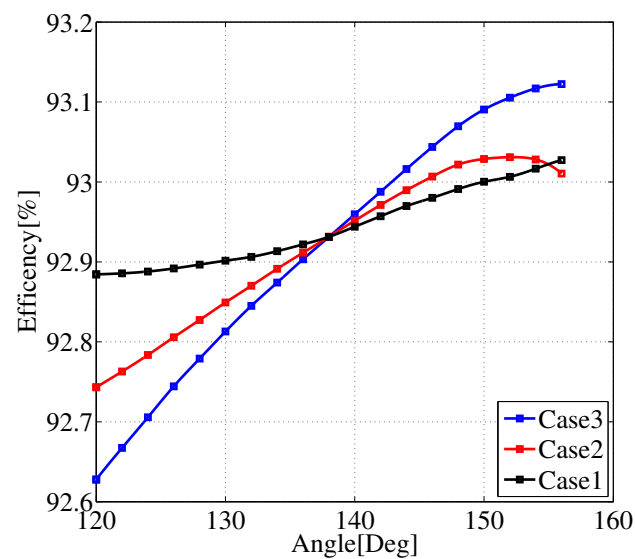


**Figure 5.28:** Efficiency in asymmetric model for different cases

The saliency ratio and the efficiency show little change compared to previous runs. The small changes for every new run is most likely a result of saturation in d-axis direction for this operation point, which have been unchanged so far. To further analyse the effect of this design on the target parameters, several different points of operation need to be evaluated.

### 5.3 SynRM Final Design - Case analysis

With the final design decided, it is interesting to analyse the behaviour of the machine for different cases. By changing the current angle  $\theta$  and the stator current magnitude,  $I_s$ , several operation points can be analysed for a fixed rotational speed. For this analysis, it is convenient to express the stator current in terms of its dq-component. With the d-q currents set between zero and a maximum of 225 A each, several different cases can be mapped. To further understand the dynamics of the performance of the machine, a look at all the target parameters is essential. The simulation output data for the different cases is demonstrated in the figures below.

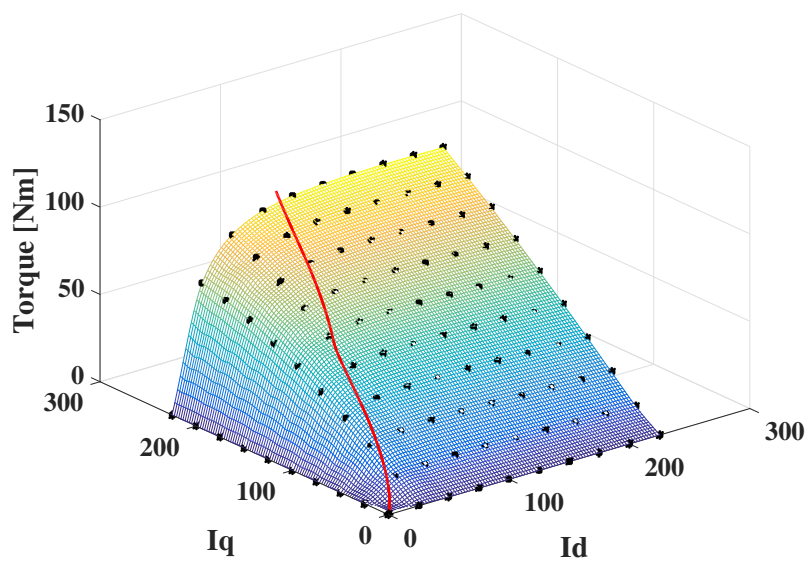


Figure 5.29: Final model torque data for different Id & Iq with MTPA line

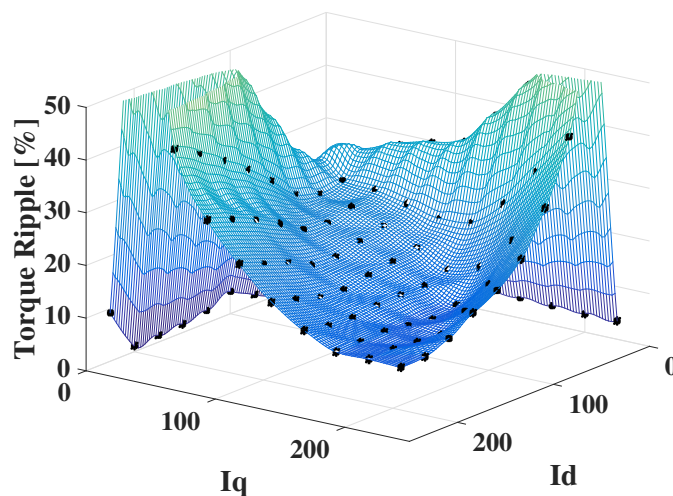


Figure 5.30: Final model torque ripple data for different Id & Iq

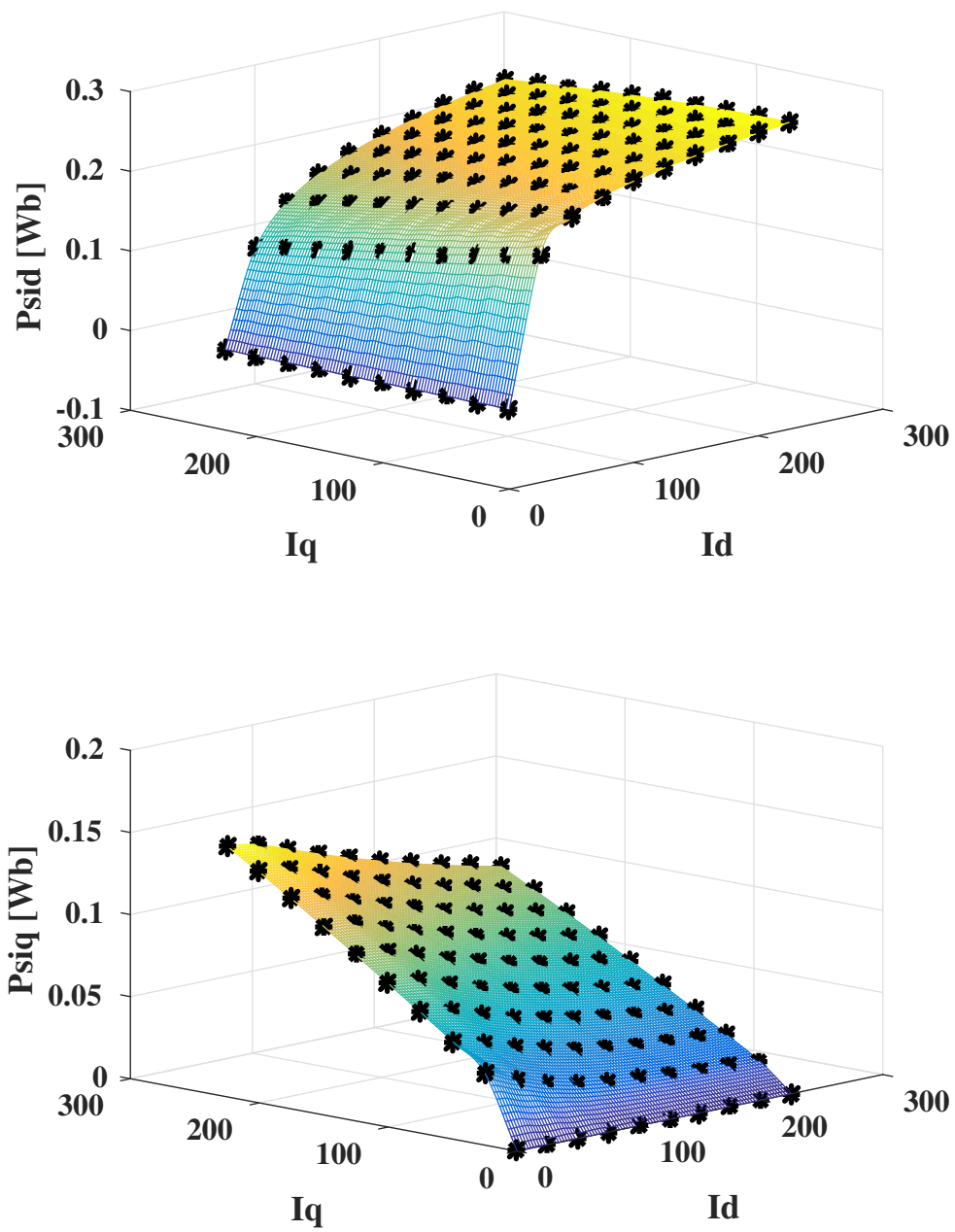


Figure 5.31: Final Model flux data for different  $I_d$  &  $I_q$

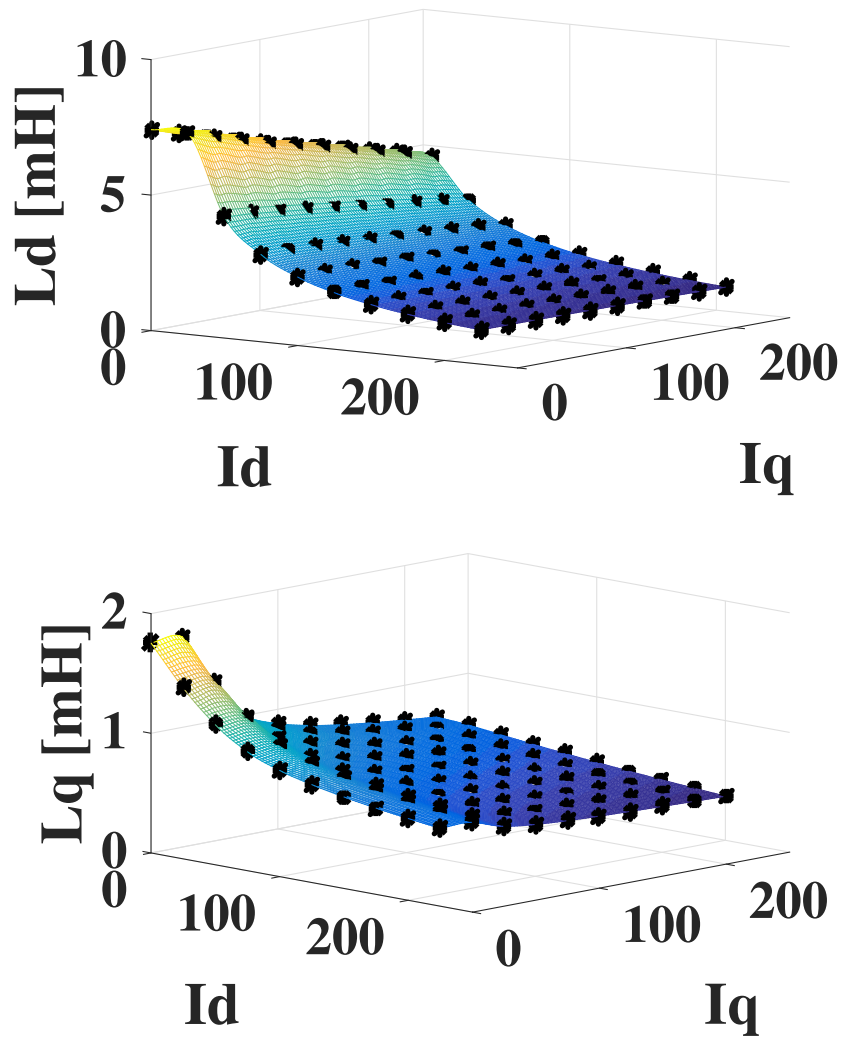


Figure 5.32: Final Model  $L_d$  &  $L_q$  data for different  $I_d$  &  $I_q$

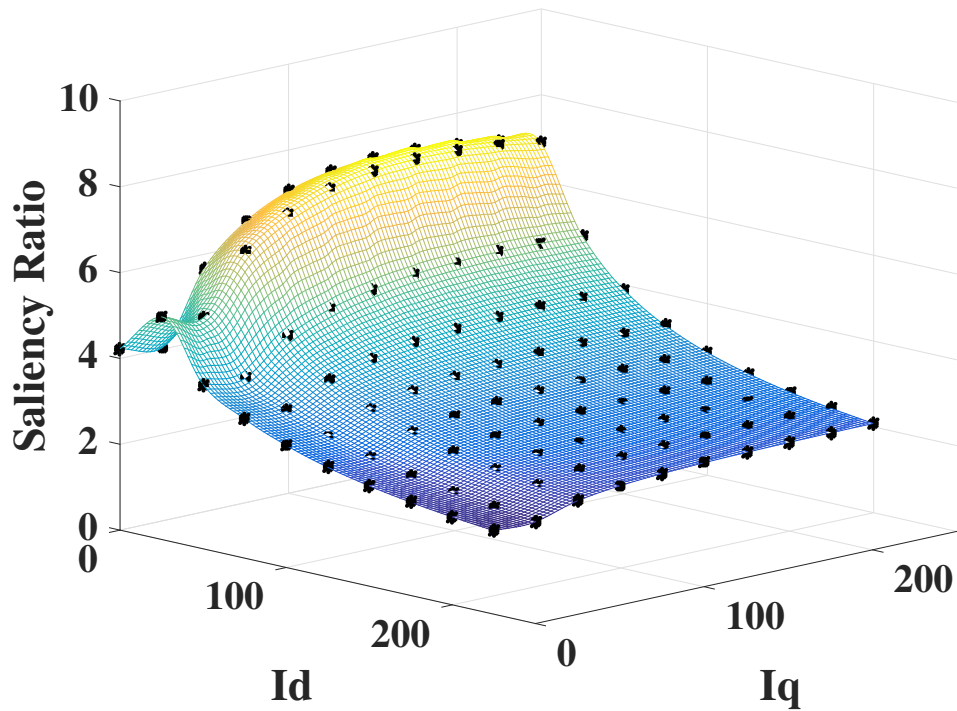


Figure 5.33: Final model saliency ratio for different Id & Iq

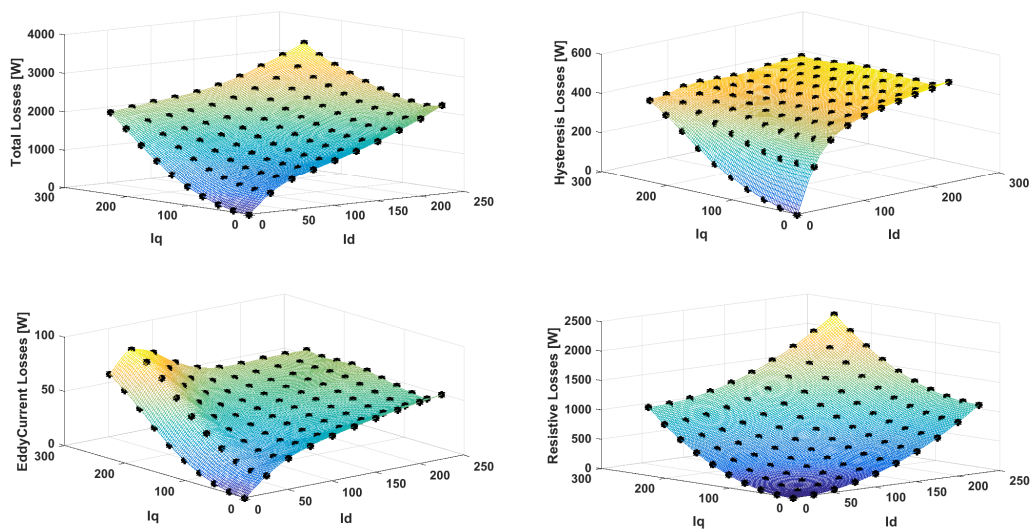
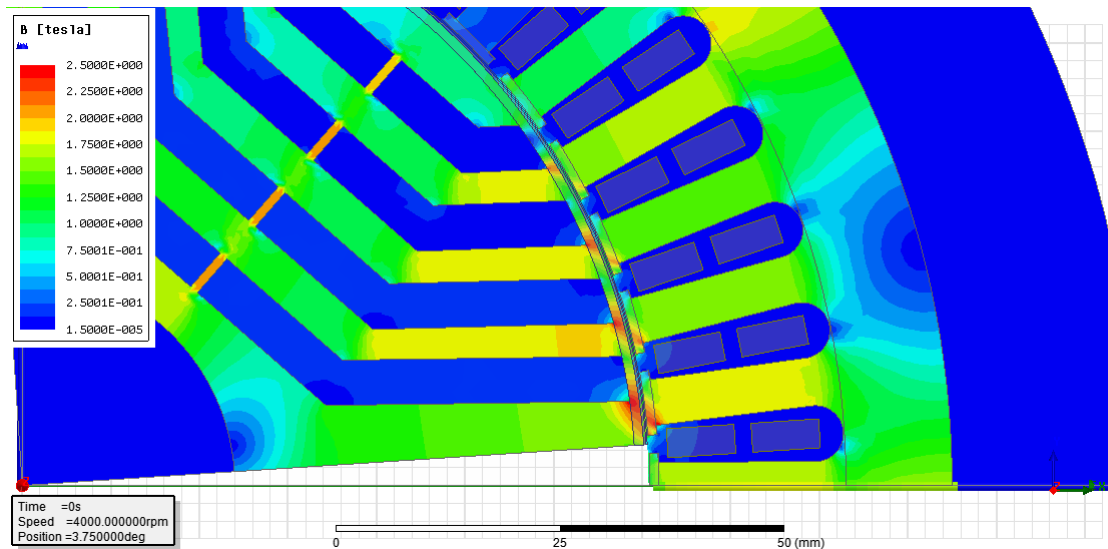


Figure 5.34: Final model Total losses, Hysteresis losses, Eddy current losses and Resistive losses for different Id & Iq

The first notable effect is the rapid decrease in saliency ratio and the d axis inductance,  $L_d$ , for increased d-axis current,  $I_d$ . Along this, a rapid saturation in the d-axis flux linkage,  $\Psi_d$ , is present as well. The q-axis inductance is also fairly high for low currents, this may be an effect of the small measurement data used to calculate the inductance near the origin. Since the flux linkage and the current are approaching zero, the inductance will increase to infinity when calculated as the ratio between flux and current. By analysing the figures above all together, it becomes clear that the saturation along the d-axis current will rapidly limit the maximum torque and the d-axis flux linkage. The resulting effect of this is a drop in the d-axis inductance  $L_d$  and therefore the saliency ratio. This also explains the low saliency ratio for all the previous simulations as well. It is however interesting to study the figures in the q-axis direction. In this direction, the dynamics are much more linear than in the d-axis directions. This is also an indication of the presence of saturation in d-direction. By studying the magnetic flux in the machine, this phenomenon can be illustrated for a selected point of operation. For a current angle of  $\theta = 45^\circ$  and a stator current of  $I_s = 221 \text{ A}$ , the magnetic flux in the machine can be seen in Fig. 5.35 below.



**Figure 5.35:** Final model magnetic flux for  $\theta = 45^\circ$ ,  $I_s = 221 \text{ A}$

In Fig. 5.35 it can clearly be seen that the saturation level is high in the iron near the air gap for the lowest two iron segments. This means that the saturation will limit the performance of the machine, no matter how much the current is being increased. Therefore, the optimum current angle is not  $45^\circ$  as in theory, if the saturation is neglected. By using the MTPA strategy, a more efficient point of operation can be found. The MTPA line can be seen in Fig. 5.29, but can be seen clearer in Fig. 5.36 below.

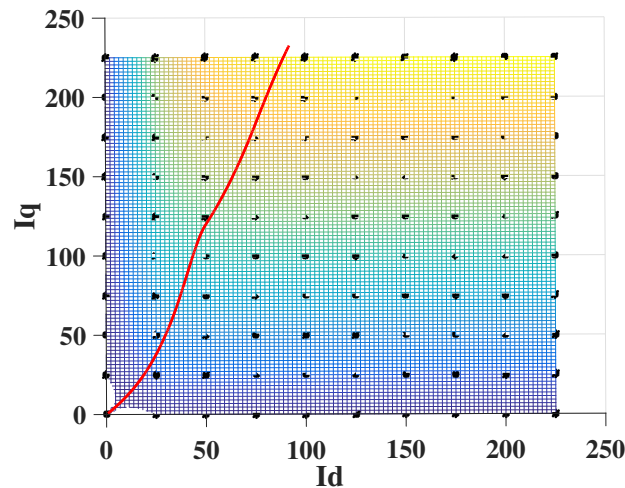


**Figure 5.36:** Final model torque with MTPA line in dq-plane

This shows that there is a possibility to reduce the d-current and still be able to achieve a somewhat identical torque compared to the in theory optimal  $45^\circ$  line. A brief look at the saliency ratio in Fig. 5.33 and the MTPA line shows that for low d-currents, the saliency remains high. A high saliency ratio is a desired effect and a high saliency ratio implies that the machine is operating at a high efficiency. Since the machine saturates quickly when the d-current increases, the MTPA line becomes more important. The correlation between the saliency ratio, saturation and MTPA line is evident. These results indicates that in order to operate this machine more efficient, a lower magnitude of the stator current and a relatively high current angle should be used. This effects clearly demonstrates the importance of proper control of the machine.

## 5.4 SynRM & PMSM comparison

The final stage of this study is to compare the PMSM against the selected design for the SynRM. Before analysing this data there are some key aspects that needs to be mentioned. First of all, the SynRM is a 4-pole machine while the PMSM is a 8-pole. As previously shown, this results in a different stator winding for the two machines, even if the same stator is being used. This means that it wont be possible to run the machines with the same current and expect the same amount of current density. As a result of this, one of these parameter should be chosen as the common parameter between the two machines in order to make the comparison as fair as possible. In this section, the machines are compared in two different cases, one where the machines have an almost identical current density an one where the machines are fed with the same current. The performance comparison is performed at different rotatinal speeds, in order to broader the analysis spectrum.

### 5.4.1 Reference - Current Density

The current density,  $J_v$ , have been calculated to approximately  $25 A/mm^2$  in the simulation setups for both machines in previous chapters. Using this data the RMS phase current in the PMSM will be  $303 A$  and  $221 A$  in the SynRM. With the current angles set to  $\theta = 135^\circ$  for the PMSM and  $\theta = 45^\circ$  for the SynRM, the obtained simulation result are demonstrated below.

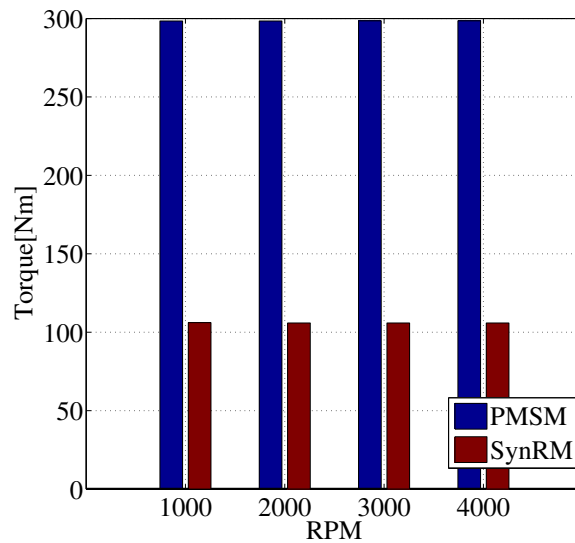


**Figure 5.37:** Average Torque in SynRM final design and PMSM for  $j_v = 25 A/mm^2$

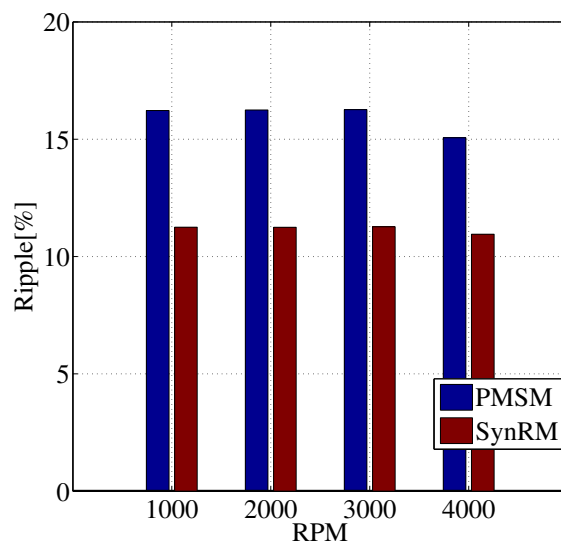


**Figure 5.38:** Torque ripple in SynRM final design and PMSM for  $j_v = 25 A/mm^2$

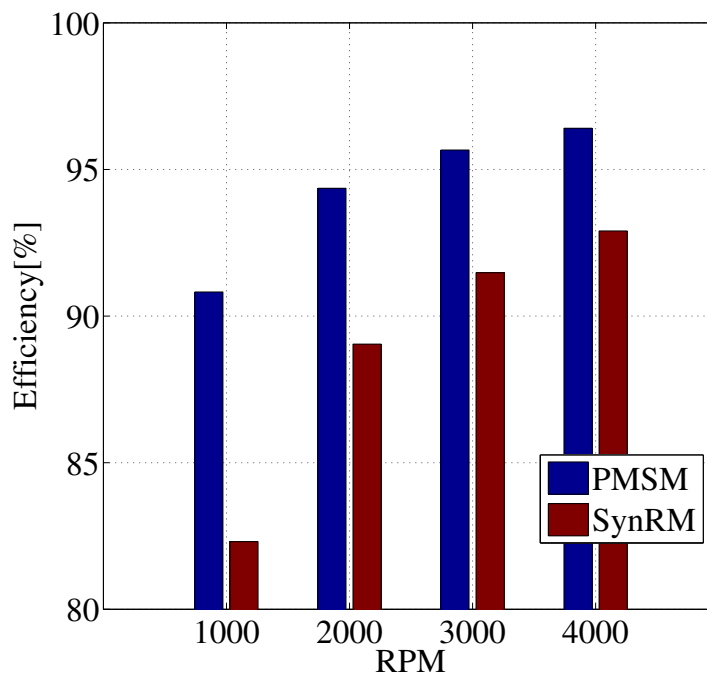


Figure 5.39: Efficiency in SynRM final design and PMSM for  $jv = 25 A/mm^2$

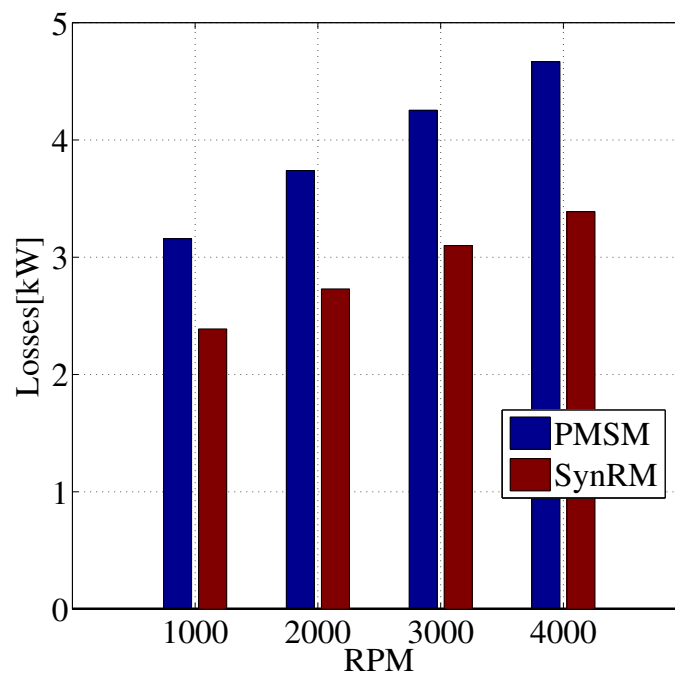


Figure 5.40: Losses in SynRM final design and PMSM for  $jv = 25 A/mm^2$

### 5.4.2 Reference - Current

The RMS phase current in the SynRM is set identical to the one in the reference motor, namely 303 A. By doing this, the SynRM will obviously have a different current density value. Having the same stator winding setup as earlier the new current density can be calculated to

$$S_{cu} = \frac{25}{4}[mm^2]$$
$$S_{cu} = 6.25[mm^2]$$

where  $S_{cu}$  is the area of one copper conductor and  $N$  is the number of turns. With a peak current that is calculated according to

$$I_{S_{peak}} = I_{S_{RMS}}\sqrt{2}[A]$$
$$I_{S_{peak}} = 420[A]$$

and two parallel branches, the current density is simply

$$J_v = \frac{420}{2 * 6.25}[A/mm^2]$$
$$J_v = 33.5[A/mm^2]$$

For obvious reasons, a higher current density means other difficulties, which will be overseen for this part of the analysis. The average torque obtained in the SynRM with the higher current is shown in Fig. 5.41 and the torque ripple in Fig. 5.42. The efficiency and the losses for the new setup are demonstrated in Fig. 5.43 and 5.44.

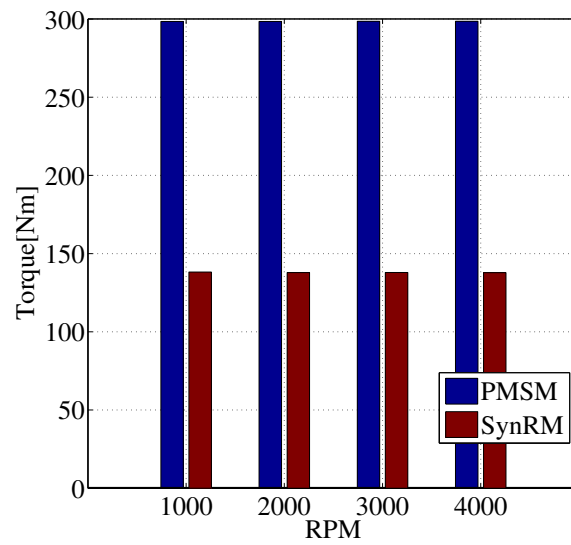


**Figure 5.41:** Average Torque in SynRM final design and PMSM for  $I_{s_{peak}} = 420$  A

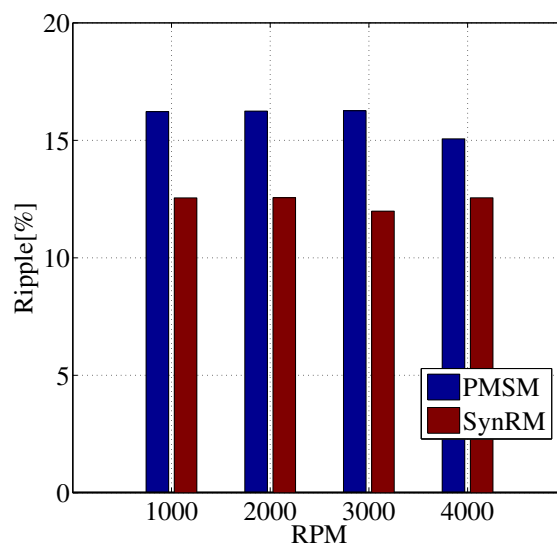


**Figure 5.42:** Torque ripple in SynRM final design and PMSM for  $I_{s_{peak}} = 420$  A

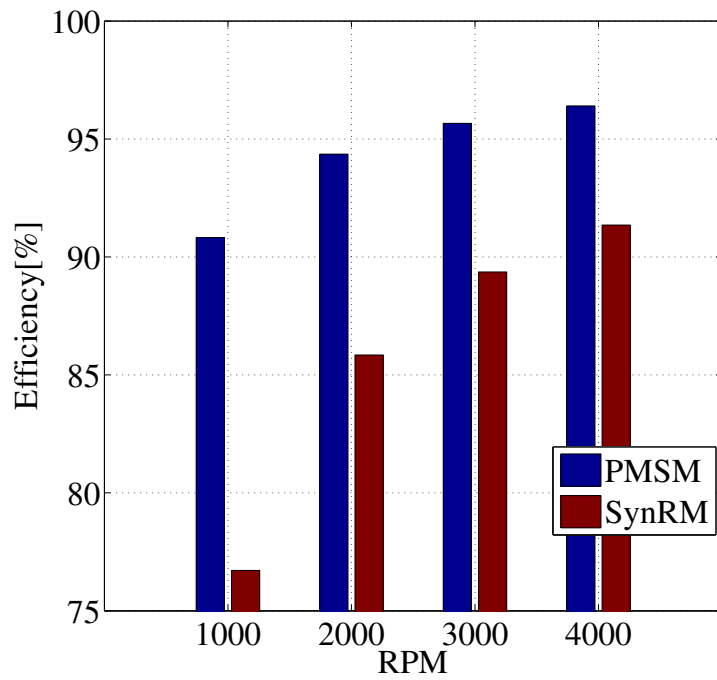


**Figure 5.43:** Efficiency in SynRM final design and PMSM for  $I_{s_{peak}} = 420 A$

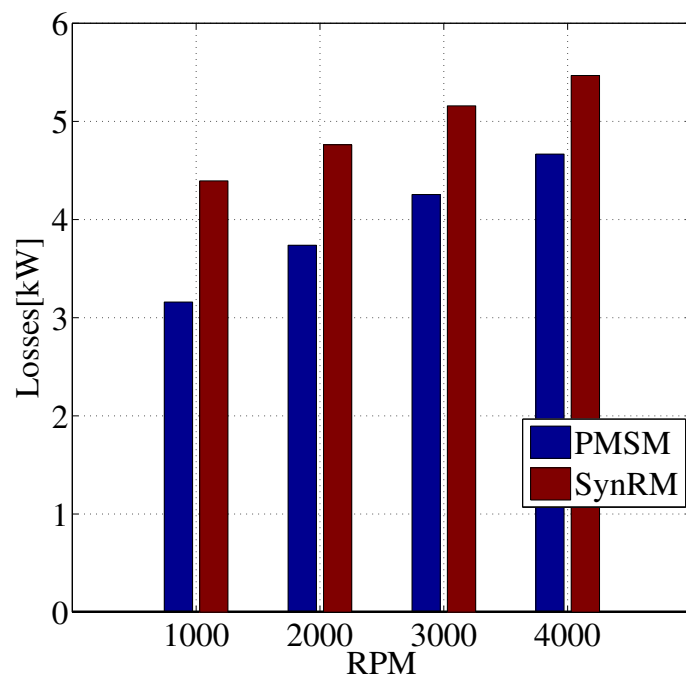


**Figure 5.44:** Losses in SynRM final design and PMSM for  $I_{s_{peak}} = 420 A$

### 5.4.3 SynRM with MTPA

One final comparison that can be useful in the comparison of the two machines is one where the SynRM is operated along the MTPA line. From the MTPA line shown in Fig. 5.29, it can be seen that one desirable point of operation is for  $I_q = 225 A$  and  $I_d = 90 A$ . Therefore, this point of operation results in that the magnitude of the peak stator current is  $I_{s,peak} = 242.33 A$  and thus results in a current angle of  $\theta = 68.2^\circ$ . This current will produce a current density of  $J_v = 19.4 A/mm^2$  which is significantly less than in both previous cases. With the PMSM being operated using the same conditions as in the two previous simulations, the difference in torque is shown in Fig. 5.45. The torque ripple, efficiency and losses with the SynRM operated along the MTPA line are respectively shown in Fig. 5.46, 5.47 and 5.48.

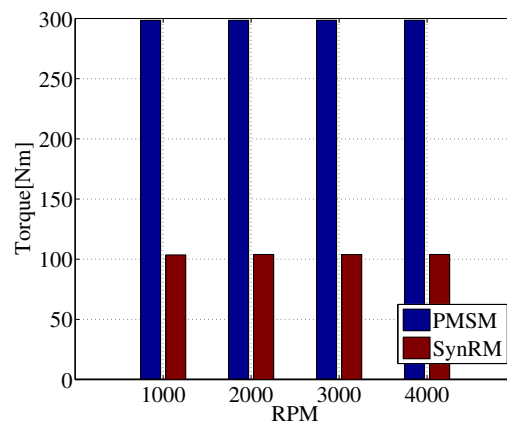


**Figure 5.45:** Average Torque in the SynRM final design at  $I_{s,peak} = 242.33 A$  and  $\theta = 68.2^\circ$

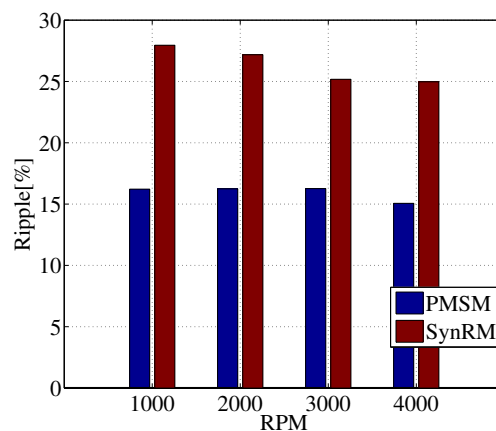


**Figure 5.46:** Torque ripple in the SynRM final design at  $I_{s,peak} = 242.33 A$  and  $\theta = 68.2^\circ$

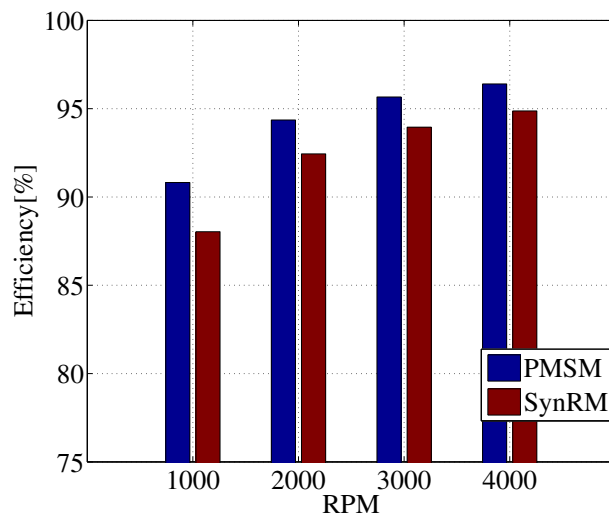


**Figure 5.47:** Efficiency in the SynRM final design at  $I_{s_{peak}} = 242.33 A$  and  $\theta = 68.2^\circ$

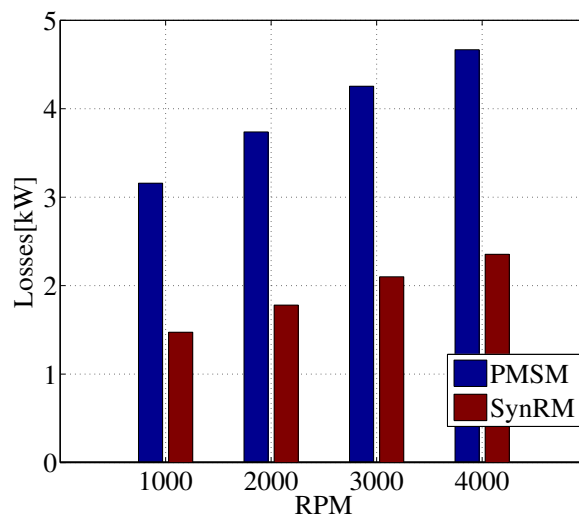


**Figure 5.48:** Losses in the SynRM final design at  $I_{s_{peak}} = 242.33 A$  and  $\theta = 68.2^\circ$

#### 5.4.4 Final Analysis

From the final simulations it can be seen that the SynRM shows significantly lower performance than the PMSM. Even if the design of the rotor is changed somewhat, this will probably only result in small changes. By running the same current density in the 4-pole SynRM against the 8-pole PMSM the loss in average torque is of a factor 3. By running the same currents in both of the machines, this factor becomes 2. In either way, the average torque is not sufficient enough to replace the PMSM in the desired application.

One interesting aspect that needs to be considered is the difference in losses and efficiency when the machine is operated along the MTPA line. As discussed earlier, the early saturation in the machine along the d-axis results in high losses and a low efficiency when the SynRM is operated along the 45° line at very high currents. By looking at the magnetic field in the SynRM rotor at 4000 *r/min* when the machine is operated at,  $I_{s,peak} = 242.33$  A, and,  $\theta = 68.2^\circ$ , some interesting differences can be seen. In Fig. 5.49 the magnetic field in the machine is displayed for this setup and the saturation level is somewhat lower in the d-axis direction, compared to earlier results presented in Fig. 5.35. However, in the direction of the q-axis, the saturation is a bit higher, which seems reasonable since the q-current is higher than in the previous case. The stator current is still relatively high but the overall level of saturation is somewhat lower. This is exactly the effect that was expected for this setup, since the previous simulations shows a higher saliency ratio in this area. But it can also be seen that even for a relatively low d-current, more specific, 90 A, the saliency ratio has already dropped and that the iron is becoming saturated in d-direction. One thing that should be pointed out is the increase in torque ripple. It have increased significantly compared to earlier simulations. However, previous simulations in this theses have shown that small changes in the air barrier angle can affect the ripple of the machine. If a point of operation is determined as an initial step, the torque ripple may be reduced by following the same procedure as have been presented earlier in Chapter 5. The relatively low current density also reduces the resistive losses and thereby the overall heat production. One of the main contributing factors to the improved efficiency of the machine at this point of operation. These results definitely indicates that the SynRM could improve its performance if the size of the machine can be increased and the current held to approximately this level. This also leads to the issue of the material of the iron in the rotor. Something that is not included in this study. By investigating how different materials for the rotor behaves in terms of saturation, maybe some of the issues with the early saturation could be eliminated.

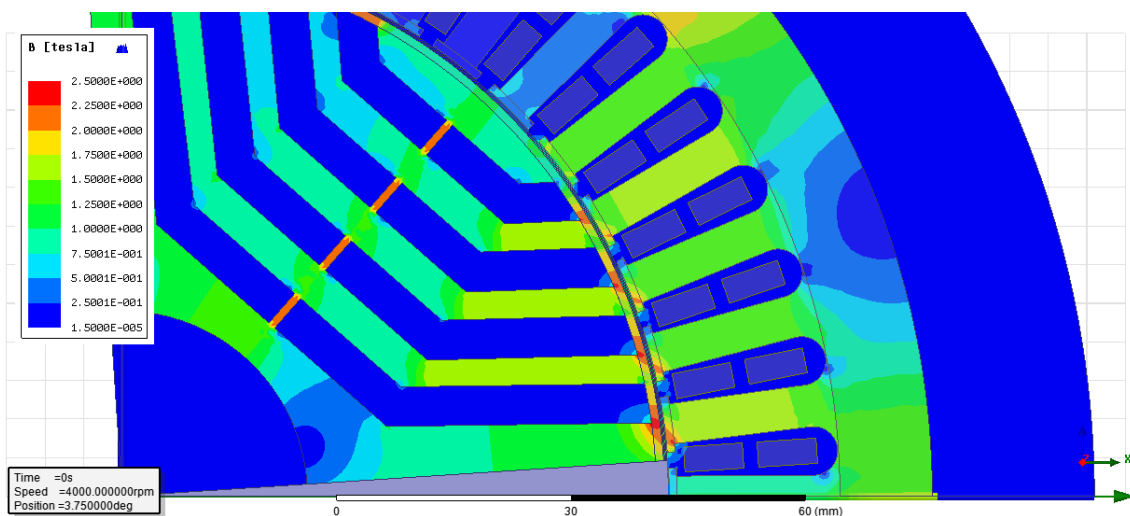


**Figure 5.49:** Magnetic field in the SynRM final design at following point of operation: 4000 *r/min*,  $I_{s,peak} = 242.33$  A and  $\theta = 68.2^\circ$

One other problem that needs to be pointed out is the fact that the comparison is done between a 4-pole and a 8-pole machine. The difference in stator windings between the two machines results in large differences in the current density. A high current density results in heat production and thereby a need for a stronger cooling system. For the same current, the SynRM runs with a current density of around  $33 \text{ A/mm}^2$  while the PMSM runs at approximately  $25 \text{ A/mm}^2$ . This while the SynRM only produces half of the torque of the PMSM. One interesting aspect is how would the results have been if the SynRM was run as a 8-pole machine. Doing this would mean different challenges and for a machine of this size, it can be discussed if this is possible or useful due to the physical restraints that this provides.

It is problematic to rule out the SynRM only based on this study. This may be an indication, but three important factors needs to be considered. Firstly, the final design of the SynRM in this study is only a suggestion, there may be more optimal ways to realize the SynRM. Secondly, the differences in pole numbers is obviously a factor which contributes to the limitations of the SynRM. One interesting study to perform would therefore be one where the sizes of the machines is increased and the pole numbers are the same. Last, the size and magnitude of the current impacts the saturation greatly. If the size of the SynRM can be increased, perhaps the saturation can be reduced even for higher currents. However, this requires a separate study.

In hybrid electric vehicle the space is often limited and the size of the machines is usually compact. Considering that for this study, the machines are meant to be used in a HEV application. This implies that one factor that can become a problem is the small air gap in the SynRM. With only 0.55 mm air gap, this may become an issue both from the manufacturing point of view and also from an operational point. Usually the motors in HEV applications operates at high speeds. With a small air gap, a study should be made to insure that the rotor does not expand to the point that the air gap becomes too small. Especially rotors with a high insulation ratio may pose a risk to this.

The overall performance of the SynRM have shown that it can not quite match the one of the PMSM. With this said, it would be useful to try out some of the other design suggestions presented in previous sections and compare these to the PMSM just to get verification. It is however expected that these changes will not have a considerable impact on the overall performance of the system.

# 6

## Conclusion

From the simulations and the analysis the study can now be concluded. In this chapter some of the main conclusions that have been made are being presented. Some suggestions on future work will also be presented in this chapter.

### 6.1 Conclusions

1. The SynRM produces approximately 55-60% less torque than the PMSM for the same current. This is achieved while it has a much higher current density in the windings compared to the PMSM. The comparison is however not entirely fair since the comparison is done between a 4-pole SynRM and an 8-pole PMSM and for an current angle that is not optimal. The torque ripple could however be reduced to as low as 12% torque ripple. The torque ripple is most dependent on the air barriers alignment against the stator teeth. Even if the design of the SynRM is improved, this will probably only result in a minor improvements of the performance and will still leave the SynRM behind the PMSM in terms of average torque.
2. The chosen design for the SynRM may not be the most optimal, but for this study it delivered expected performance. Since all of the presented SynRM design presents similar performance and characteristics, a more extensive study could be needed. The peak to peak ripple increases as the modeling constant  $jk$  decreases, but the minimum values for the ripple are therefore lower. The insulation ratio plays a important role for the performance of the machine. The chosen value for the insulation ratio was  $Kwq = 0.8$  since higher values than this started to show an inverted trend. This can at this stage however not be concluded. A more extensive study could be needed to investigate how even higher insulation ratios impact the machine.
3. The saliency ratio drops rapidly as the d-current increases. This, mainly due to a rapid saturation in the d-axis direction and thus a decrease in d-axis inductance  $L_d$ . If the rapid saturation that occurs can be eliminated, the result will most probably be an increase in torque, d-inductance, saliency ratio and therefore an improvement of overall performance.
4. When the machine was operated along the MTPA line it showed significant improvement in terms of efficiency and reduced losses. This is due to the lower

saturation of the iron in the rotor. This shows on how important control of the machine actually is. The torque ripple increased at this point of operation. However, the ripple could probably be reduced by adjustment of the air barrier angles. With an increased size of the SynRM, it would perhaps be able to handle larger currents and still maintain an efficiency level on with the PMSM.

5. At this stage, the results indicates that the SynRM is not a viable replacement for the reference PMSM in HEV application. If the size of the SynRM can be increased, this may not be the case. Before the SynRM is completely ruled out as an option in HEV application, some further study related to the design of the SynRM need to be performed.

## 6.2 Future Work

There are some interesting aspects of this study that needs more in depth analysis in a eventual future study. Some of these aspects are presented below.

1. To study insulation ratios above 1 in the SynRM to see if there is a major impact of this parameter to the overall performance of the machine.
2. Since the saturation in d-axis is high, one interesting study would be to see if it can be lowered for the same point of operation using an increase in rotor diameter. It would be useful to see how the overall performance of the machine will change if the size of the machine is increased and the material of the rotor is changed.
3. For machines out of this size, making 8-pole SynRM may become problematic due to the limitation of space in the rotor. It would however be very interesting to see if any improvement to the overall performance could be gained by doing so. It would also be a more fair comparison to the reference PMSM.
4. The Mathematical Model 1 used in this study is a somewhat simplified version of the original presented in [6]. By applying the original theory, maybe the overall performance of the SynRM would be improved.

# Bibliography

- [1] P. Niazi, H. A. Toliyat and A. Goodarzi, "Robust Maximum Torque per Ampere (MTPA) Control of PM-Assisted SynRM for Traction Applications," in IEEE Transactions on Vehicular Technology, vol. 56, no. 4, pp. 1538-1545, July 2007. doi: 10.1109/TVT.2007.896974
- [2] Anon (2016) Arafura - Pricing. Online Available at: <http://www.arultd.com/rare-earths/pricing> (accessed 16/ 05/ 16).
- [3] Anon (2016) Arafura - Supply & Demand. Online Available at: <http://www.arultd.com/rare-earths/supply-demand.html> (accessed 16/ 05/ 16).
- [4] J.K Kostko, Polyphase Reaction Synchronous Motors, Journal of the American Institute of Electrical Engineers Vol. 42 (No. 11) 1162-1168.
- [5] T. A. Lipo (1991) Synchronous Reluctance Machines-A Viable Alternative for AC Drives, Electric Machines and Power Systems, 19:6, 659-671.
- [6] R.R Moghaddam, Synchronous reluctance machine (SynRM) Design, Master thesis, The Royal Institute of Technology, KTH (2007).
- [7] Malan.J;Kamper, M.J.; Williams, "Reluctance synchronous machine drive for hybrid electric vehicle," in Industrial Electronics, 1998. Proceedings. ISIE '98. IEEE International Symposium on , vol.2, no., pp.367-372 vol.2, 7-10 Jul 1998
- [8] Emeka S. Obe and A. Binder (2009) Calculation of Rotor Currents of Single-phase Synchronous Reluctance Motor Using d-q Harmonic Balance Techniques, Electric Power Components and Systems, 37:9, 943-956
- [9] P.Tokat, Design and Evaluation of a Permanent Magnet Generator for Wave Power Applications, Licentiate Thesis, Chalmers University of Technology , CTH, (2015)
- [10] A. Kiltbau, J. M. Pacas, "Appropriate Models for the Control of the Synchronous Reluctance Machine," Conference Record of the 2002 IEEE Industry Applications Conference, 37th IAS Annual Meeting and World Conference on Industrial Applications of Electrical Energy, vol. 4, pp. 2289 – 2295.

- [11] Yammine, S.; Henaux, C.; Fadel, M.; Desharnais, S., Synchronous reluctance machine flux barrier design based on the flux line patterns in a solid rotor, in *Electrical Machines (ICEM)*, 2014 International Conference on , vol., no., pp.297-302, 2-5 Sept. 2014
- [12] Guan, Y.; Zhu, Z.Q.; Afinowi, I.A.A.; Mipo, J.C.; Farah, P., "Design of synchronous reluctance and permanent magnet synchronous reluctance machines for electric vehicle application," in *Electrical Machines and Systems (ICEMS)*, 2014 17th International Conference on , vol., no., pp.1853-1859, 22-25 Oct. 2014
- [13] R.R Moghaddam, Synchronous Reluctance Machine (SynRM) in Variable Speed Drives (VSD) Applications, PhD thesis, The Royal Institute of Technology, KTH (2011).
- [14] Wang, K.; Zhu, Z.Q.; Ombach, G.; Koch, M.; Zhang, S.; Xu, J., "Optimal slot/pole and flux-barrier layer number combinations for synchronous reluctance machines," in *Ecological Vehicles and Renewable Energies (EVER)*, 2013 8th International Conference and Exhibition on , vol., no., pp.1-8, 27-30 March 2013
- [15] Vartanian, R.; Toliyat, H.A.; Akin, B.; Poley, R., "Power factor improvement of synchronous reluctance motors (SynRM) using permanent magnets for drive size reduction," in *Applied Power Electronics Conference and Exposition (APEC)*, 2012 Twenty-Seventh Annual IEEE , vol., no., pp.628-633, 5-9 Feb. 2012
- [16] Kamper, M.J., "Effect of rotor dimensions and cross magnetisation on  $L_d$  and  $L_q$  inductances of reluctance synchronous machine with cageless flux barrier rotor," in *Electric Power Applications*, IEE Proceedings - , vol.141, no.4, pp.213-220, Jul 1994
- [17] S.Taghavi, Design of Synchronous Reluctance Machines for Automotive Applications, PhD Thesis, Concordia University (2015)
- [18] Staton, D.A.; Miller, T.J.E.; Wood, S.E., "Maximising the saliency ratio of the synchronous reluctance motor," in *Electric Power Applications*, IEE Proceedings B , vol.140, no.4, pp.249-259, July 1993
- [19] Loubser, A.T.; Kamper, M.J., "Design optimisation of reluctance synchronous machine for drive system efficiency," in *Electrical Machines Design, Control and Diagnosis (WEMDCD)*, 2015 IEEE Workshop on , vol., no., pp.60-65, 26-27 March 2015
- [20] Ju Hui Mun; Jae Sub Ko; Jung Sik Choi; Mi Geum Jang; Dong Hwa Chung, "Efficiency optimization control of SynRM Drive using multi-AFLC," in *Electrical Machines and Systems (ICEMS)*, 2010 International Conference on ,

vol., no., pp.908-913, 10-13 Oct. 2010

- [21] Liang Yan-ping; Liu Jin-peng; Chen Jing, "Calculation of iron loss and stray losses for high-voltage induction motor using time-stepping finite element method," in *Mechanic Automation and Control Engineering (MACE)*, 2010 International Conference on , vol., no., pp.4081-4084, 26-28 June 2010
  
- [22] Yicheng Chen; Pillay, P., "An improved formula for lamination core loss calculations in machines operating with high frequency and high flux density excitation," in *Industry Applications Conference, 2002. 37th IAS Annual Meeting. Conference Record of the* , vol.2, no., pp.759-766 vol.2, 13-18 Oct. 2002
  
- [23] C. H. Hong, H. c. Liu, H. S. Seol, H. W. Jun and J. Lee, "Decrease torque ripple for SynRM using barrier arrangement design," *Electrical Machines and Systems (ICEMS)*, 2014 17th International Conference on, Hangzhou, 2014, pp. 1834-1837.

